Supplemental Document

Toward high-gain laser-driven electron undulators: supplement

AMNON BALANOV, RON RUIMY, AND IDO KAMINER*

Department of Electrical and Computer Engineering, Technion–Israel Institute of Technology, Haifa 3200003, Israel
kaminer@technion.ac.il

Supplement DOI: https://doi.org/10.6084/m9.figshare.28303460

Parent Article DOI: https://doi.org/10.1364/OPTICA.540401

Toward high-gain laser-driven electron undulators

Amnon Balanov, Ron Ruimy and Ido Kaminer*

Department of Electrical and Computer Engineering, Technion – Israel Institute of Technology, Haifa 3200003, Israel

*corresponding author: kaminer@technion.ac.il

Supplemental Document

Contents

1. Introduction

In this section, we briefly introduce the electron micro-bunching physical process and review the notations used throughout this work. Figure S1 describes the micro-bunching process. It includes three components: the electron beam, the counter-propagating laser beam, and the co-propagating X-ray wave. We assume the counter-propagating laser beam is linearly polarized. The axes notation used in this work are: 1) the z-axis is the electron beam velocity direction. 2) The x-axis is the laser's beam electric field direction and the undulation motion of the electrons in the self-frame. 3) the y-axis is the laser's beam magnetic field direction. Table S1 shows the notation used throughout the paper. It includes the parameters of the electron beam, the counter-propagating laser beam, the FEL parameters, and the X-ray beam.

The FEL facilities include two categories of gain mechanisms: the low-gain FEL and the high-gain FEL [6]. In the low-gain FEL, the electron beam passes multiple times in a low-gain medium. After many passes, the X-ray wave power exponentially increases until it reaches saturation. Despite significant recent progress, this approach is limited by the X-ray optical components and the required electron source repetition rate. In contrast, in the high-gain regime, the electron beam passes only once in a long-gain medium. The transverse electric field of the X-ray radiation interacts with the transverse electron current such that some electrons gain, and others lose energy to the X-ray field through the ponderomotive force. When the X-ray radiation becomes sufficiently strong, it modulates the electrons' longitudinal velocity and focuses electrons into bunches shorter than the X-ray wavelength. These bunches act as single particles with high charge, creating collective emission, enhancing the radiation intensity to be quadratic in the electron bunch charge rather than linear as in the incoherent regime (see Figure S1 for illustration). This phenomenon is unique to the high-gain FEL and does not occur in other X-ray sources, leading to the extremely high-brightness X-ray pulses that are unique to FELs.

The micro-bunching process includes the following steps: 1) The counter-propagating laser beam applies EM forces on the electron beam, generating undulation motion of the electrons in the x-axis. 2) The electrons' oscillations produce a linear polarized X-ray beam, co-propagating with the electron beam in the z-direction. 3) The generated X-ray beam applies an additional force on the electron bunch pulse. Combining the co-propagating X-ray wave and the counter-propagating laser beam creates a first order standing wave, in addition to the zero-order EM field of the counter-propagating laser. 4) The electron undulation in the x-axis creates forces in the z-direction (due to the magnetic field applied to the electron beam in the y-axis). Since the electrons' undulation oscillation strength depends on z (in the first order standing wave approximation), electrons will modulate toward the regions with lower electric fields (i.e., this is the ponderomotive force).

The supplementary material includes the following sections: Section 2 describes the incoherent inverse Compton scattering (ICS) scheme, including the incoherent ICS spatial dispersion, cross-section, and spectral density profile. In Section 3, we review the general

requirements of the high-gain ICS, particularly the electron source requirements. In Section 4, we derive the laser source requirements and bounds for the laser pulse duration, power, beam waist, and energy. In Section 5 we derive the upper bounds of the high-gain ICS peak brightness and saturation power, assuming an electron source that achieves the 6D quantum-mechanical brightness bound. In section 6, we analyze state-of-the-art and near-future electron and laser sources and discuss the experimental feasibility of implementing a high-gain scheme in the Extreme UV (EUV) and water-window spectrum. In section 7, we analyze the performance of the low-gain ICS (the ICS oscillator) and compare it with the high-gain scheme concerning allowed linewidth broadening, quantum-recoil effects, and scaling of the emission energy.

	Parameter	Description	Units
Electron beam	$E_{\mathrm{e}} = \gamma_{\mathrm{e}} m_{\mathrm{e}} c^2$	Electron beam energy.	MeV
	$\Delta\gamma_{\mathrm{e}}/\gamma_{\mathrm{e}}$	Electron beam energy spread.	-
	$\frac{\sigma_E}{E}$	Electron beam effective energy spread, which accounts also spread due to divergence.	-
	ϵ_n	Electron beam normalized emittance.	nm-rad
	$\sigma_{\mathrm{e}}^2 = \sigma_x \sigma_y$	The electron beam spot size at interaction point (RMS).	$\mu\mathrm{m}^2$
	$\sigma_{x'}, \sigma_{y'}$	The electron beam divergence at interaction point (RMS).	mrad^2
	β_{av}	Average beta function of the electron beam.	m
	I_{e}	The electron beam peak current.	A
	n_{e}	The electron charge density.	$1/\mathrm{m}^3$
	$B_{n,e}$	The Electron beam brightness.	$\frac{\mathrm{C}}{\mathrm{s\ mm^2\ mrad^2}}$
Counter-propagating laser beam	λ_L	The laser wavelength.	μm
	$\Delta\lambda_L/\lambda_L$	The laser linewidth.	-
	N_L	Number of photons within a pulse.	-
	E_0	Electric field amplitude.	GV/m
	K , a_0	Undulator parameter, normalized vector potential.	-
	σ_L^2, $w_0^{(L)}$	Laser spot size at interaction point, beam waist	μm
	$z_R^{(L)}$	Rayleigh length.	m
	I_0	Laser pulse intensity.	$\mathrm{W/cm^2}$
	P_0	Laser pulse power.	GW
	$\tau_{\mathrm{p}}^{(L)}$	Laser pulse duration.	ps
	$E_{\mathrm{p}}^{(L)}$	Laser pulse energy	J
FEL	ρ_{FEL}	The Pierce\FEL parameter.	-
	Γ	FEL gain parameter.	$1/\mathrm{m}$
	L_{g0}	FEL gain length.	m
	L_{sat}, L_g	Saturation length / interaction length	m
	k_p	Space charge length	$1/\mathrm{m}$
	N_u	Number of undulation periods.	-
X-ray beam	λ_x	Wavelength	μm
	B_n	Peak brightness	$\frac{\mathrm{photons}}{\mathrm{s\ mm^2\ mrad^2\ 0.1\%BW}}$
	P_{sat}	Saturation power	W

Table S1: The high-gain ICS parameters which are used through the work.

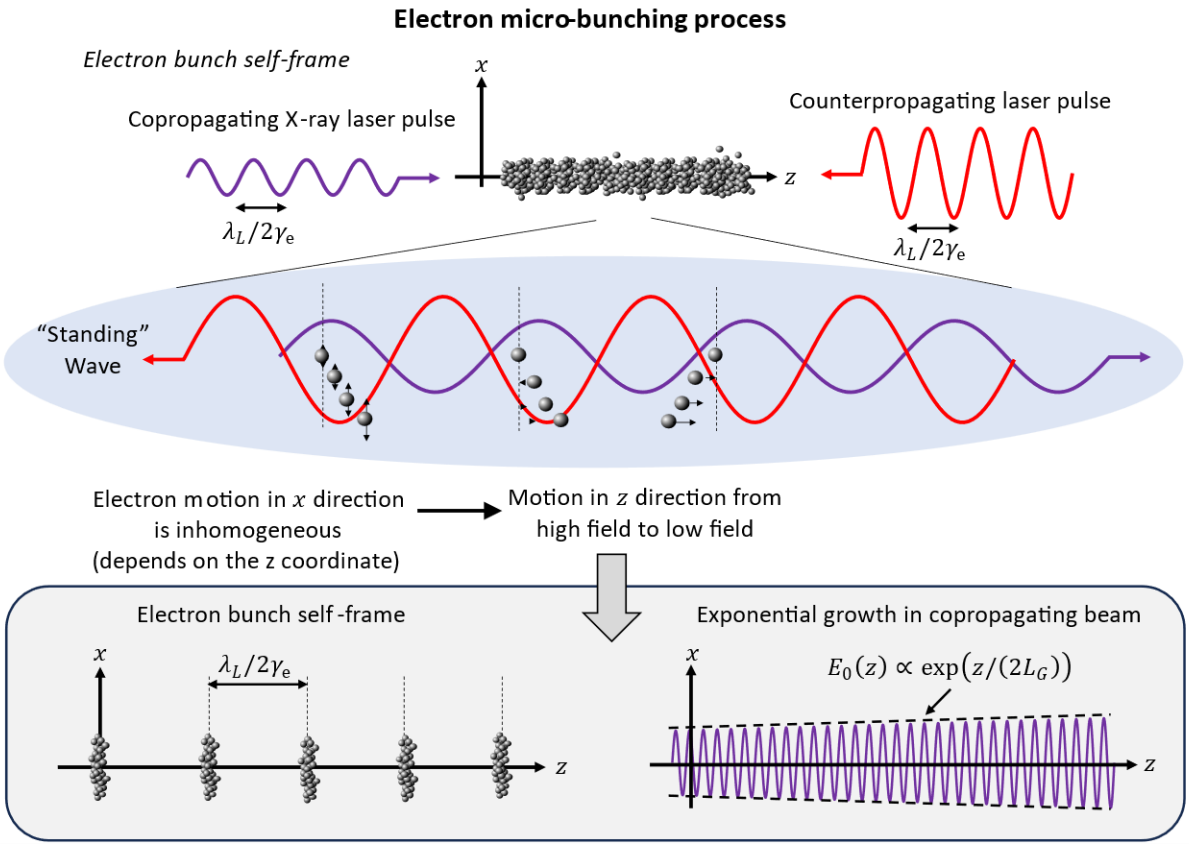

Figure S1: The micro-bunching process. **(a)** The scheme composes the electron beam, the counter-propagating micrometer laser pulse, and the co-propagating X-ray laser pulse. When looking at the electrons' self-frame, both the counter-propagating and the co-propagating X-ray beam have wavelengths of $\frac{\lambda_L}{2\gamma_e}$ (arising due to the Doppler shift). Their sum can be thought of as a combination of a standing wave (from the first order) and an additional plane wave (from the zero-order). As the sum of the waves creates an inhomogeneous electric field (i.e., the standing wave is periodic in $z = \lambda_L/2\gamma_e$), the electrons' oscillations in the x-axis depend on the location of the electrons in the wavelength period. The electrons' transverse motion (x-axis) creates longitude oscillations (z-axis) due to the magnetic field applied to the electron beam. This phenomenon is the pondermotive force. This results in an electron modulation toward the regions where the electric field is minimal, generating bunches with the periodicity of the emission wavelength. **(b)** The micro-bunching process creates electron bunches separated by a distance of $\frac{\lambda_L}{2\gamma_e}$ (in the self-frame). The micro-bunching process leads to an exponential growth of the X-ray beam, which scales as $\propto \exp\left(z/\left(2L_{g0}\right)\right)$, where L_{g0} is the FEL gain length.

2. Background

2.1 The inverse Compton scattering scheme

Inverse Compton Scattering is the up-conversion process of a low-energy laser photon to a high-energy X-ray photon by scattering from a relativistic electron. Figure S2(a) shows the interaction scheme with a near-head-on collision between the laser and electron beams. The scattered X-rays emerge in the same direction as the electrons. The physical mechanism of ICS is nearly identical to spontaneous synchrotron emission in a static magnetic undulator as used in traditional synchrotron facilities. However, due to the much shorter micro-meter laser wavelength, relative to the centimeter-period undulator wavelength, the required electron energies to produce hard X-ray photons are orders of magnitude lower than in the large synchrotrons. The up-conversion ratio for low laser intensity and on-axis emission from a head-on collision is given by [1][2] [3]:

$$\lambda_x \approx \lambda_L(1+\gamma_e^2\theta^2)/4\gamma_e^2\,, \tag{S1}$$

where θ is the X-ray photon emission angle relative to the electron beam direction, λ_L is the laser wavelength and λ_x is the emitted X-ray wavelength. The total ICS flux over all angles and frequencies is determined by the cross-section between the electron beam and the laser photons and is given by:

$$N_x = \frac{N_e N_L \sigma_T}{2\pi(\sigma_L^2+\sigma_e^2)}, \tag{S2}$$

where σ_T is the Thomson cross section, N_e is the total number of electrons, N_L is the total number of photons in the laser beam, and σ_L and σ_e are the beam spot size at the interaction point of the laser and electron beam, respectively. The up-conversion ratio (Eq. (S1)) implies that all photons emitted within a narrow cone of $\sim 0.1\gamma_e^{-1}$ have an energy linewidth of 1%. Figure S2(a) shows the ICS parabolic spatial dispersion emission profile [2]. One should note that Eq. (S1) is similar to the up-conversion ratio of synchrotron radiation where $\lambda_u = \lambda_L/2$. The difference between them rises due to the Lorentz transform in the synchrotron case versus the Doppler shift in the ICS case.

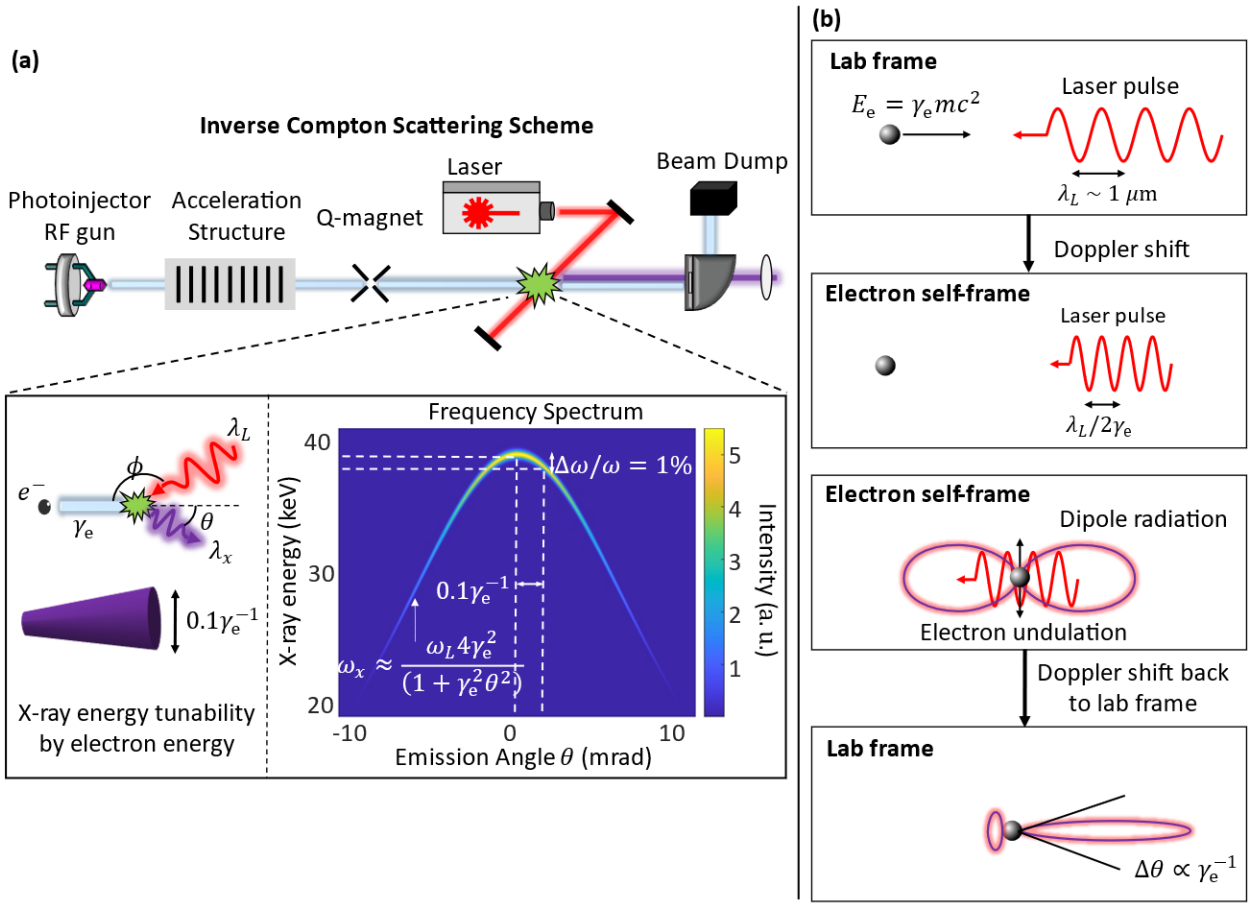

Figure S2: Background on inverse Compton scattering. **(a)** Incoherent inverse Compton scattering X-ray source scheme. A relativistic electron beam collides head-on with a laser pulse, upconverting the laser photon energy to an X-ray photon. Within a narrow emission cone $\sim 0.1\gamma_e^{-1}$ in the forward direction, the X-ray beam energy linewidth is 1%. **(b)** The physical process of inverse Compton scattering. In the Lab frame, the counterpropagating laser pulse has a wavelength of λ_L. In the electron's self-frame, the laser wavelength is $\lambda_L/2\gamma_e$ due to Doppler shift, assuming a head-on collision. The laser EM field undulates the electrons, producing dipole-shaped radiation with a wavelength of $\lambda_L/2\gamma_e$. Back to the lab frame, the dipole-shaped radiation is concentrated due to Doppler shift, producing directional emission into the forward direction with an emission cone proportional to γ_e^{-1} and a central wavelength of $\lambda_L/4\gamma_e^2$.

2.2 Spatial dispersion and the X-ray linewidth

The X-ray beam brightness in FEL facilities reaches much higher levels than synchrotrons due to the electron micro-bunching and the resulting coherent emission. The central requirement for fulfilling electron micro-bunching is that the co-propagating X-ray beam energy linewidth would be below the Pierce parameter (known also as the FEL parameter) [4]. As the co-propagating X-ray beam linewidth depends on the electron source and laser beam quality parameters, we review the spatial dispersion of the ICS scheme and derive the electron and laser source requirements for fulfilling successful micro-bunching. To obtain some intuition, the spatial dispersion emission of the ICS process is examined [2]:

$$\lambda_x(\theta) = \frac{\lambda_L}{2\gamma_e^2(1-\beta\cos\phi)}\left(1+(\gamma_e\theta)^2+\frac{K^2}{2}\right), \tag{S3}$$

where $\lambda_L = 2\lambda_u$ is the ICS laser wavelength, γ_e is the Lorentz factor of the electron, β is the electron velocity, θ is the emission angle relative to the electron trajectory, ϕ is the angle between the electron and the laser photon ($\phi = \pi$ for heads-on collision). K is the undulator parameter, given by:

$$K = \frac{eE_0\lambda_L}{2\pi m_e c^2}, \tag{S4}$$

where E_0, B_0 are the electric and magnetic fields of the laser, respectively, m_e is the electron mass and c is the speed of light. Typical parameters in ICS schemes are laser wavelengths of $\lambda_L \sim 1-10$ μm (near infrared (NIR) to long wave infrared (LWIR)), electron beam energy of 5-40 MeV and an undulator parameter of $K < 0.1$ (in the linear regime of ICS). For the case of relativistic electron beam $\gamma_e \gg 1$, head-on collision $\phi = \pi$ and $K < 0.1$, Eq. (S3) can be approximated by Eq.(S1).

A crucial parameter for the electron micro-bunching is the X-ray emission energy spread, as specified by Eq. (S3). In particular, the electron energy spread and emittance, as well as the laser beam intensity fluctuations, determine the energy spread of the emitted X-ray. The broadening of these parameters is derived directly from Eq. (S3):

$$\left(\frac{\Delta\lambda_x}{\lambda_x}\right)_{\text{energy spread}} = 2\frac{\Delta\gamma_e}{\gamma_e}, \tag{S5}$$

$$\left(\frac{\Delta\lambda_x}{\lambda_x}\right)_{\text{emittance}} = \gamma_e^2\theta^2 = \frac{\epsilon_{xn}^2}{\sigma_x^2}, \tag{S6}$$

$$\left(\frac{\Delta\lambda_x}{\lambda_x}\right)_{\text{laser fluctuations}} = \frac{K^2\frac{\Delta K}{K}}{1+\frac{K^2}{2}}, \tag{S7}$$

$$\left(\frac{\Delta\lambda_x}{\lambda_x}\right)_{\text{laser linewidth}} = \frac{\Delta\lambda_L}{\lambda_L}, \tag{S8}$$

The first term (Eq. (S5)) describes the X-ray linewidth spread due to the electron source energy spread. The electron energy spread in state-of-the-art undulator FEL electron sources is $10^{-4} - 10^{-3}$, while an order below for Ultrafast Electron Microscope (UEM) electron sources ($10^{-5} - 10^{-4}$) [5]. The second term is the electron beam emittance (Eq. (S6)). This term arises due to electron beam divergence, which increases the effective electron energy spread. Thus, low electron emittance sources are necessary to fulfill this condition. The third term (Eq. (S7)) describes the energy spread due to the laser beam fluctuations (Figure 3(b) + (c) in the main text). The laser beam fluctuation originates from two phenomena: 1) the laser intensity fluctuates over time (i.e., intensity noise). 2) The laser beam divergence. The typical requirements for the laser intensity fluctuations are a few percentages, whereas the requirements for the laser beam divergence are defined through its Rayleigh length. The Rayleigh length should be much longer than the interaction length for a negligible effect on the X-ray energy broadening. The fourth term (Eq. (S8)) describes the X-ray linewidth due to the laser beam linewidth. We assume during this work that the laser systems are optimized to the Fourier-limit pulse duration; thus, the laser linewidth (or, equivalently, the coherence length) is derived directly from the laser pulse duration.

Assuming the collisions are heads-on, such that $\phi = \pi$ and that the scheme is the linear ICS regime, i.e., $K \ll 1$, the X-ray wave energy spread can be represented by:

$$\frac{\Delta\omega_x}{\omega_x}\Big|_{\theta=0} = \sqrt{\left(2\frac{\Delta\gamma_{\text{e}}}{\gamma_{\text{e}}}\right)^2 + \left(\frac{\epsilon_{xn}^2}{\sigma_x^2}\right)^2 + \left(K^2\frac{\Delta K}{K}\right)^2 + \left(\frac{\Delta\lambda_L}{\lambda_L}\right)^2}, \tag{S9}$$

To fulfill the conditions for micro-bunching, the X-ray linewidth described by Eq. (S9) should be below the Pierce parameter, i.e., $\Delta\omega_x/\omega_x < \rho_{\text{FEL}}$. Figure 3 in the main text demonstrates these artifacts. The first two terms (the electron beam terms) will be further discussed in section 3, while the last two terms (the laser beam terms) will be further discussed in section 4.

2.3 Incoherent inverse Compton scattering cross-section and spectral density

In this section, we describe the incoherent ICS cross-section and spectral density. We assume head-on collisions and relativistic electron energies $\gamma_e \gg 1$. For this case, the emitted X-ray photon spectral density flux produced by a single electron is given by [2]:

$$\frac{d^2N_{se}(\theta,\omega)}{d\Omega d\omega} = \frac{d\sigma}{d\Omega}(\theta,\phi)\sqrt{\frac{2}{\pi}}\frac{1}{\Delta\omega_0|g(\theta)|}\exp\left\{-\frac{2(\omega-\omega_0|g(\theta)|)^2}{\Delta\omega_0^2|g(\theta)|^2}\right\}\int F_{\omega_0}(t)dt \ , \quad \text{(S10)}$$

where $\hbar\omega$ is the emission energy, θ is the emission angle, $\frac{d\sigma}{d\Omega}$ is the cross-section between the electron beam and the laser beam, $F_{\omega_0}(t)$ is the laser photon flux temporal profile, $g(\theta)$ is the spatial dispersion relation between the emission angle and energy (Eq. (S12)), ω_0 is the laser angular frequency and $\Delta\omega_0$ is the effective linewidth, which considers all the four terms in Eq. (S9), i.e.:

$$\frac{\Delta\omega_0}{\omega_0} = \left.\frac{\Delta\omega_x}{\omega_x}\right|_{\theta=0}$$

The cross-section between the electron and lasers beams is given by:

$$\frac{d\sigma}{d\Omega}(\theta,\phi) \approx r_e^2\frac{4\gamma_e^2}{(1+\gamma_e^2\theta^2)^2}\left(1-\frac{4\gamma_e^2\theta^2}{(1+\gamma_e^2\theta^2)^2}\sin^2\phi\right), \quad \text{(S11)}$$

where r_e is the electron radius, and ϕ is the angle between the electron beam to the laser beam. The spatial dispersion $g(\theta)$ is given by:

$$g(\theta) = \frac{4\gamma_e^2}{(1+\gamma_e^2\theta^2)}, \quad \text{(S12)}$$

which is the dispersion relation as specified in Eq. (S1). Therefore, $\Delta\omega_0|g(\theta)|$ represents the emitted X-ray energy spread as a function of the emission angle. The laser photon flux $F_{\omega_0}(t)$ is given by:

$$F_{\omega_0}(t) = c\left(1-\frac{c}{\omega_0}\boldsymbol{\beta_e}\cdot\boldsymbol{k_0}\right)n_\gamma[r_e(t),t], \quad \text{(S13)}$$

where n_γ is the photons pulse density.

The typical incoherent ICS spectral density is shown in Figure S2(a). The emission spectrum has a parabolic shape specified by Eq.(S1), with spectral density emission angle dependence as specified by Eq. (S10). The energy linewidth at $\theta = 0$ is described by Eq. (S9). The typical energy linewidth for ICS sources is 1% [3]. Assuming the pulse density is constant over time, and the pulse duration is τ_{pulse}, then:

$$\int F_{\omega_0}(t)dt = \frac{c\epsilon_0|E_0|^2}{2}\tau_{\text{pulse}}\frac{1}{\hbar\omega_0}$$

Therefore, the spectral density flux for a single electron is:

$$\frac{d^2N_{\text{se}}(\theta,\omega)}{d\Omega d\omega} \approx \frac{r_{\text{e}}^2}{(1+\gamma_{\text{e}}^2\theta^2)\Delta\omega_0}\frac{c\epsilon_0|E_0|^2}{2}\tau_{\text{pulse}}\frac{1}{\hbar\omega_0}\exp\left\{-\frac{2(\omega-\omega_0|g(\theta)|)^2}{\Delta\omega_0^2|g(\theta)|^2}\right\}$$

And the spectral density energy is:

$$\frac{d^2I_{\text{se}}(\theta,\omega)}{d\Omega d\omega} = \frac{d^2N_{\text{se}}(\theta,\omega)}{d\Omega d\omega}\hbar\omega = \frac{r_{\text{e}}^2}{(1+\gamma_{\text{e}}^2\theta^2)\Delta\omega_0}\frac{c\epsilon_0|E_0|^2}{2}\tau_{\text{pulse}}\frac{\hbar\omega}{\hbar\omega_0}$$

Since $\frac{\hbar\omega}{\hbar\omega_0} = g(\theta)$, the spectral density energy is derived to be:

$$\frac{d^2I_{\text{se}}(\theta,\omega)}{d\Omega d\omega} = \frac{4\gamma_{\text{e}}^2r_{\text{e}}^2}{(1+\gamma_{\text{e}}^2\theta^2)^2\Delta\omega_0}\frac{c\epsilon_0|E_0|^2}{2}\tau_{\text{pulse}}\exp\left\{-\frac{2(\omega-\omega_0|g(\theta)|)^2}{\Delta\omega_0^2|g(\theta)|^2}\right\}, \qquad \text{(S14)}$$

The maximal value of the spectral density energy for $\theta = 0$ and $\omega = \omega_0|g(\theta)|$ is:

$$\max\left\{\frac{d^2I_{\text{se}}(\theta,\omega)}{d\Omega d\omega}\right\} = \frac{4\gamma_{\text{e}}^2r_{\text{e}}^2}{\Delta\omega_0}\frac{c\epsilon_0|E_0|^2}{2}\tau_{\text{pulse}}$$

As we will see in the next sections, the main advantages of the high-gain ICS over the incoherent ICS are the lower emission linewidth (the energy linewidth, $\Delta\omega_x/\omega_x$, is at least an order of magnitude lower), smaller emission cone ($\sqrt{\rho_{\text{FEL}}}\gamma_{\text{e}}^{-1}$ instead of γ_{e}^{-1}), and larger number of photons produced per electron. Overall, the coherent high-gain ICS brightness will be 5-8 orders of magnitude higher than the incoherent ICS scheme.

3. The high-gain inverse Compton scattering

Before diving into the FEL parameters and requirements that determine the condition for high-gain ICS, we summarize the main conditions of the electron and laser sources.

3.1 Electron beam requirements

The electron beam quality (i.e., beam energy, emittance, energy spread, and focusing) has a crucial impact on the performance of the high-gain regime. Table S1 shows the parameters that define the electron beam quality.

Electron beam spot size, divergence, and beta function

On the one hand, the electron beam should be focused into a small spot size to increase the charge density, resulting in stronger ponderomotive forces and more effective micro-bunching. On the other hand, focusing the beam too much will increase the beam divergence, which will enlarge the effective energy spread (Figure 3(a) in the main text). Moreover, the beam spot size will spread much faster, limiting the maximal interaction length. The electron's beam beta function captures this tradeoff. The beta function $\beta_{x,y}(z)$ is analogous to the Rayleigh length of a laser beam, i.e., when the electron beam goes through distance $\beta_{x,y}$ from the beam waist, the beam spot size increases by a factor of σ_x^2. Thus, the beta function sets the effective interaction length for the electron beam [2]. It is defined by:

$$\sigma_x^2(z) = \epsilon_x \beta_x(z), \qquad \sigma_y^2(z) = \epsilon_y \beta_y(z), \tag{S15}$$

where ϵ_x, ϵ_y are the beam emittance at the transverse plane, and σ_x, σ_y are the beam spot size (RMS). We will assume the beam has a circular shape such that $\beta_x = \beta_y$, $\epsilon_x = \epsilon_y$ and the beta function position dependence is negligible. We denote the average beta function by $\beta_{\mathrm{av}} = \overline{\beta_x(z)} = \overline{\beta_x(z)}$. To preserve a focused electron beam along the interaction length, the average beta function should be larger than the interaction length, i.e., $\beta_{\mathrm{av}} \geq \frac{1}{2} L_{\mathrm{sat}}$. Due to the much shorter saturation length of the high-gain ICS compared with the undulator FEL, the possible ICS high-gain beta function is much lower than the one of the undulator FEL: in the undulator FEL, the typical beta function is 5-30m, while for the high-gain ICS, it is below 10 cm. A noticeable difference between the undulator FEL and the high-gain ICS is that in FEL facilities, the undulator is split into separate sections, in which the electron beam is focused after each section [6]. In contrast, in the high-gain ICS scheme, we analyze the scenario where no additional focusing elements exist along the short interaction length. Moreover, the electron beam spot size of the high-gain ICS scheme is much smaller than the undulator FEL: for the undulator FEL, it is ~100μm, while for the high-gain ICS, it is a few micrometers. One should note that from the requirements on the electron beam divergence (Eq. (S6)), the following holds:

$$(\gamma_{\mathrm{e}} \sigma_{x'})^2 \leq \frac{1}{2} \rho_{\mathrm{FEL}} \rightarrow \frac{\gamma_{\mathrm{e}}^2 \epsilon}{\beta_{\mathrm{av}}} \leq \frac{1}{2} \rho_{\mathrm{FEL}} \rightarrow \epsilon \leq \frac{1}{2} \frac{\rho_{\mathrm{FEL}} \beta_{\mathrm{av}}}{\gamma_{\mathrm{e}}^2}$$

Figure 3(d) in the main text shows this requirement on the beta function of the electron beam. Due to the dependence of the Pierce parameter on the electron pulse density (Eq. (S20)), the electron pulse density should be at least ~$10^{21} - 10^{22}\,\frac{1}{\mathrm{m}^3}$ for an effective generation of the X-ray wave and for creating electron micro-bunching. The charge density requirement, combined with the required electron beam emittance, sets a requirement on the electron source normalized brightness and on the scaling laws for the allowed X-ray energies of the high-gain ICS scheme (Figure 4(a) in the main text).

Electron beam emittance

The electron beam emittance is approximately the product between the electron beam spot size and beam divergence, i.e. [6]:

$$\epsilon_x = \sigma_x \sigma_{x'}, \qquad \epsilon_y = \sigma_y \sigma_{y'}$$

As mentioned previously, we assume $\epsilon_x = \epsilon_y$. We will use throughout this work the electron normalized-emittance metric, defined by $\epsilon_n = \gamma_\mathrm{e}\epsilon_x$, as it is Lorentz-transform invariant [7]. A low electron beam emittance is a crucial requirement for the high-gain ICS scheme. The electron beam emittance is related to a few aspects of the micro-bunching process. First, it defines the beta function and the electron beam spot size (Eq. (S15)). Second, the electron beam divergence affects the X-ray energy spread (Eq. (S6)); thus, a low beam emittance allows lower energy spread. Third, the electron beam emittance defines the emitted X-ray spatial (transverse) coherence. The diffraction limit of a Gaussian beam with a wavelength λ_x is given by $\lambda_x/4\pi$. Therefore, to achieve the diffraction limit requirement, the electron beam emittance should satisfy [4]:

$$\epsilon = \frac{\epsilon_n}{\beta\gamma_\mathrm{e}} = \sigma_x \sigma_{x'} < \frac{\lambda_x}{4\pi}, \tag{S16}$$

The condition set by Eq. (S16) captures all the three requirements above. For a high-gain ICS scheme, the electron beam normalized emittance should be much lower than the one of an undulator FEL due to the inverse dependence on the electron energy, i.e., $\epsilon \propto \gamma_\mathrm{e}^{-1}$. For example, for an emission wavelength of $\lambda_x = 5$Å, the undulator FEL requires normalized beam emittance of $\epsilon_n \approx 500\,\mathrm{nm\,rad}$, while the high-gain ICS with a laser wavelength of $\lambda_L = 1\mu\mathrm{m}$ requires normalized electron beam emittance of $\epsilon_n \approx 1\,\mathrm{nm\,rad}$. Therefore, the electron pulse charge used in undulator FEL is higher than in high-gain ICS scheme, yet due to the larger focusing in the high-gain ICS, the electron charge density (n_e) is approximately the same between the two schemes. Overall, the required electron beam emittance restricts the number of electrons within a pulse, but not the electron charge density. Therefore, the expected brightness gain of the coherent ICS relative to the incoherent ICS will be lower than the gain between synchrotron (incoherent electrons emission) and FEL facilities (coherent electrons emission) due to the quadratic X-ray intensity scaling as a function of the number of electrons within a bunch (N_e^2). Figure 2(c) in the main text shows the required electron beam normalized emittance.

It is important to emphasize that the condition set by Eq. (S16) is necessary for a fully coherent beam but is stricter than the conditions for the electron micro-bunching process to occur. Figure 2(c) in the main text shows the dependence between the X-ray wavelength and the required normalized emittance for a fully coherent ICS scheme. One should note electron energy dependence in Eq. (S16): due to the $\lambda_x \propto \gamma_e^{-2}$ dependence, the normalized emittance should be lower for higher X-ray energies ($\epsilon_n \propto \lambda_x \gamma_e \propto \frac{\lambda_u}{\gamma_e}$). These requirements are very demanding and can't be met with current electron source technology for hard X-rays. However, they can be met for the soft X-ray spectrum (< 2 keV).

Electron beam energy spread

From Eq. (S5), the electron beam energy spread is an additional factor that significantly impacts the high-gain ICS scheme. Since the Pierce parameter for the high-gain ICS is an order of magnitude below the undulator FEL, the electron beam energy spread in the high-gain ICS scheme should be an order of magnitude below the undulator FEL. The typical value for the required electron energy spread is $10^{-5} - 10^{-4}$.

3.2 Counter-propagating laser beam requirements

The laser beam quality (i.e., beam intensity, power, duration, energy, Rayleigh length, spot size, and linewidth) is crucial for satisfying the conditions for micro-bunching, as specified by Eq. (S7) and Eq. (S8). We will find the bounds of these parameters in section 4. Here, we present the intuition about the requirements of these parameters.

Laser beam intensity and fluctuations

On the one hand, for a strong interaction between the electron and laser beams, the undulator parameter (K) should be as high as possible. On the other hand, a high undulator parameter will cause a linewidth broadening due to the laser fluctuations (Eq. (S7)), resulting in non-linear effects [2]. Therefore, the electric field strength is limited by the X-ray linewidth broadening requirement. Typically, the laser's electric field strength should be in the range of tens GV/m for long-wave infrared (LWIR) laser and a few ~hundreds of GV/m for near infrared (NIR) laser.

In addition, the laser intensity fluctuations after stabilization should be low since the emission linewidth depends on the laser intensity noise. If the laser intensity fluctuations cannot be met, then a lower undulator parameter should be used. Figures 3(b) and (c) in the main text show this artifact.

Laser beam spot size, divergence and Rayleigh length

The laser spot size should be much larger than the electron beam spot size for a uniform electric field strength applied on the electrons in the transverse plane. Typically, the beam spot size should be a few hundred micrometers. In addition, the laser Rayleigh length should be much longer than the interaction length. This requirement is necessary since the laser intensity should be uniform along the whole longitude axis of the interaction. i.e., the laser beam divergence should be small enough in the interaction point. In section 4.5 we discuss these requirements, as well as the M^2 paramter of the laser beam.

Laser beam linewidth and pulse duration

The laser linewidth should be smaller than the Pierce parameter (Eq. (S8)). Equivalently, the coherence length should be longer than the interaction length. We will assume the laser system is optimized for the transform-limited pulse duration; thus, the laser pulse length should be as long as a few tens (~20) FEL gain length periods for the electron micro-bunching [4]. Typically, it should be up to a few hundred picoseconds. The exact conditions for the electron source will be discussed in the following sections.

3.3 Mathematical description

In this section, we review the high-gain regime requirements. Specifically, we review the FEL parameters and the FEL requirements for electron micro-bunching. We will show further below that the FEL equations are similar between a magnetic undulator and a coherent ICS scheme. Therefore, we adopt the FEL parameters and use the FEL conditions for the coherent ICS scheme. In addition to the FEL requirements, we derive additional requirements for the coherent ICS in the following sections.

The main difference between the undulator FEL and the coherent ICS is due to the much shorter undulation period (centimeter versus micrometer), the lower electron beam energy (a few tens MeV versus > 10GeV), and the lower electron beam emittance, which together put strict requirements for the micro-bunching process. In addition, the conditions on the laser beam are challenging. In this section, however, we will not analyze them, as we will assume the laser beam is "ideal", i.e., the laser beam is uniform along the interaction length, it has high enough power, negligible divergence, and linewidth, and its spot size is much larger than the electron beam spot size.

The electron micro-bunching process is based on the interaction between the electron beam, the counter-propagating laser beam, and the co-propagating X-ray beam. The process involves first the creation of the X-ray wave due to the undulation motion of the electrons. Then, the interaction between the X-ray wave and the electron beam modulates the electron velocities due to the ponderomotive force, resulting in an electron micro-bunching with the periodicity of the X-ray

wavelength (Figure S1). To describe the micro-bunching process, one needs to consider the motion of each electron using the relativistic Newtonian equations of motion, together with the Maxwell equations for the X-ray beam generation and amplification. The equations are similar between the high-gain FEL and the high-gain ICS, with the main differences of counter-propagating laser instead of the undulator and the different energy scales. We will use the derivation of the high-gain FEL and specify the differences relative to the ICS. First, let us donate the problem variables as specified in Table S2.

#	Parameter	Description
1	N_{e}	The number of electrons in the pulse
2	$\boldsymbol{r_i}, \boldsymbol{p_i}$	The position and momentum of the i-th electron ($1 \leq i \leq N_{\mathrm{e}}$)
3	$\boldsymbol{E}^{(L)}$, $\boldsymbol{B}^{(L)}$	The electric and magnetic fields of the counter-propagating beam (the ICS laser beam).
4	$\boldsymbol{E}^{(X)}$, $\boldsymbol{B}^{(X)}$	The electric and magnetic fields of the co-propagating beam (the X-ray beam).
5	$\rho(\boldsymbol{r})$	The total charge density of the electron beam.
6	$\boldsymbol{j}(\boldsymbol{r}, t)$	The total current density of the electron beam.

Table S2: Notations used to describe the micro-bunching process in the high-gain FEL regime.

For each electron $1 \leq i \leq N_e$, the equations of motion are governed by the Lorentz force applied by the counter-propagating laser wave and the co-propagating X-ray wave:

$$\begin{aligned} \frac{d\boldsymbol{p_i}}{dt} &= \frac{d(\gamma_{\mathrm{e}} m \boldsymbol{v_i})}{dt} \\ &= e\left[\left(\boldsymbol{E}^{(L)}(\rho, z, t) + \boldsymbol{v_i} \times \boldsymbol{B}^{(L)}(\rho, z, t)\right)\right. \\ &\left. + \left(\boldsymbol{E}^{(X)}(\rho, z, t) + \boldsymbol{v_i} \times \boldsymbol{B}^{(X)}(\rho, z, t)\right)\right] \end{aligned} \tag{S17}$$

where $\boldsymbol{E}^{(L)}(\rho, z, t)$, $\boldsymbol{B}^{(L)}(\rho, z, t)$ represent the co-propagating laser's EM field, and $\boldsymbol{E}^{(X)}(\rho, z, t)$, $\boldsymbol{B}^{(X)}(\rho, z, t)$ represent the copropagating X-ray beam. One should note that the laser's EM field is determined by the external laser beam, while the X-ray wave is generated during the process and is dynamically changed with the propagation in the z axis. The equations of motions are accompanied by the Maxwell equations that describe the generation and amplification of the X-ray beam:

$$\begin{aligned} \nabla \cdot \boldsymbol{E}^{(X)} &= \frac{\rho}{\epsilon_0} \\ \nabla \cdot \boldsymbol{B}^{(X)} &= 0 \\ \nabla \times \boldsymbol{E}^{(X)} &= -\frac{\partial \boldsymbol{B}^{(X)}}{\partial t} \\ \nabla \times \boldsymbol{B}^{(X)} &= \mu_0 \left(\boldsymbol{j} + \epsilon_0 \frac{\partial \boldsymbol{E}^{(X)}}{\partial t}\right) \end{aligned} \tag{S18}$$

where in the case at hand, the density charge and current density are set by the electron bunch charge:

$$\begin{aligned} \rho(\boldsymbol{r}) &= \sum_i q_i \delta(\boldsymbol{r} - \boldsymbol{r_i}) \\ \boldsymbol{j}(\boldsymbol{r}, t) &= \sum_i q_i \boldsymbol{v}_i(t) \delta(\boldsymbol{r} - \boldsymbol{r_i}) \end{aligned} \tag{S19}$$

We briefly describe the physical process: First, the external laser field ($\boldsymbol{E}^{(L)}$, $\boldsymbol{B}^{(L)}$) generates forces on the electron, resulting in an undulation motion in the x-axis (p_x) and a weaker harmonic motion in the z-axis (p_z) (Eq. (S17)). The undulation motion creates changes in the current density j_x, generating a radiation field (the X-ray wave ($\boldsymbol{E}^{(X)}$, $\boldsymbol{B}^{(X)}$)) with a wavelength equal to the undulation periodicity (Eq. (S18d)). The generated X-ray wave creates forces on the electrons (Eq. (S17), the last term). These forces modulate the electron charge density ($\rho(\boldsymbol{r})$) in the z-axis, such that they create an effective electric field in the z-axis E_z (Eq. (S18a)). Therefore, the X-ray wave interaction with the electron beam creates micro-bunching, while the repulsion between the electrons opposes the process. If the X-ray wave force on the electrons is larger than the repulsion between the electrons, then micro-bunching will occur.

Eq. (S17)-(S19) are a set of partial differential equations with $6N + 1$ equations of motion for each electron. In the general case, this set of equations is not analytically solvable, and numerical tools are used to solve it [6]. However, under the assumption of the 1D theory and the slowly varying amplitude approximation (SVA), these equations set coupled first-order differential equations. These equations are further simplified by the assumption that the periodic density modulation remains small, resulting in a third-order differential equation containing only the electric field amplitude. The last simplification derives an analytically solvable set of equations. The analytic solution to these equations shows that the electric field increases exponentially with the FEL gain length.

In this section, we review the FEL parameters which impact the performance of the micro-bunching process. We will include in the discussion the updates needed for the coherent ICS process due to the electron energy spread and emittance. However, we will neglect the laser fluctuation, i.e., we assume the laser is uniform over the interaction length. In the next section, we will discuss the laser fluctuation term and its impact in detail.

3.4 The FEL parameters

The Pierce parameter

The Pierce parameter (or FEL parameter) is a central parameter in the FEL mechanism, defining the X-ray beam emission linewidth, the maximal output beam power, and the condition of the energy spread of the electron source. It is given by [4]:

$$\rho_{\mathrm{FEL}} = \frac{1}{2}\left(\frac{\pi K^2 r_{\mathrm{e}} n_{\mathrm{e}}}{k_u^2 \gamma_{\mathrm{e}}^3}\right)^{\frac{1}{3}}, \tag{S20}$$

where K is the undulator parameter, r_{e} is the electron radius, n_{e} is the electron pulse density, $k_u = \frac{2\pi}{\lambda_u}$ and γ_{e} is the electron energy. The electron pulse density is given by:

$$n_{\mathrm{e}} = \frac{Q_{\mathrm{e}}}{e\tau_{\mathrm{p}} c\, \pi r_b^2}, \tag{S21}$$

where Q_{e} is the pulse charge, τ_{p} is the pulse duration, c is the speed of light, e is the electric charge, and r_b is the electron beam radius.

The Pierce parameter is typically in the range of $\sim 10^{-4} - 10^{-3}$ in FEL facilities (smaller values correspond to hard X-rays while larger values correspond to soft X-rays). For the coherent ICS case, the Pierce parameter is about an ~order smaller than an FEL undulator (Figure 2(b) in the main text); therefore, the electron source should have an order lower energy spread (including the energy spread due to the emittance term). Figure S3(a) shows the impact of the electron charge density on the Pierce parameter. The Pierce parameter increases for denser electron charges and shorter X-ray wavelengths. A higher Pierce parameter implies less strict requirements on the electron energy spread and emittance, yet at the expanse of higher X-ray beam linewidth. Another dependence of the Pierce parameter is on the electric field strength ($\rho_{\mathrm{FEL}} \propto K^{2/3} \propto E_0^{2/3}$), i.e., larger values of the laser electric fields will increase the Pierce parameter. However, increasing the electric field (and consequently the laser power) will come at the expense of higher laser fluctuations and non-linear effects. We will discuss this trade-off in the next section.

The FEL gain length

Additional parameters which are related to the Pierce parameter are the FEL gain parameter Γ and the power gain length L_{g0} [4]:

$$\Gamma = \frac{4\pi\rho_{\mathrm{FEL}}}{\lambda_u}, \tag{S22}$$

$$L_{g0} = \frac{1}{\sqrt{3}\Gamma} = \frac{\lambda_u}{4\pi\sqrt{3}\rho_{\mathrm{FEL}}}, \tag{S23}$$

These parameters define the typical length scale of the exponential increase in power of the emitted X-ray beam. Figure S3 in the main text compares the power gain length between the FEL scheme and the coherent ICS scheme as a function of the emitted X-ray wavelength. The power gain length of the ICS scheme is more than three orders lower than the power gain length of the FEL scheme, which shows the promising prospects of shrinking the ~100m undulator length to a few tens centimeters length of the high-gain ICS scheme.

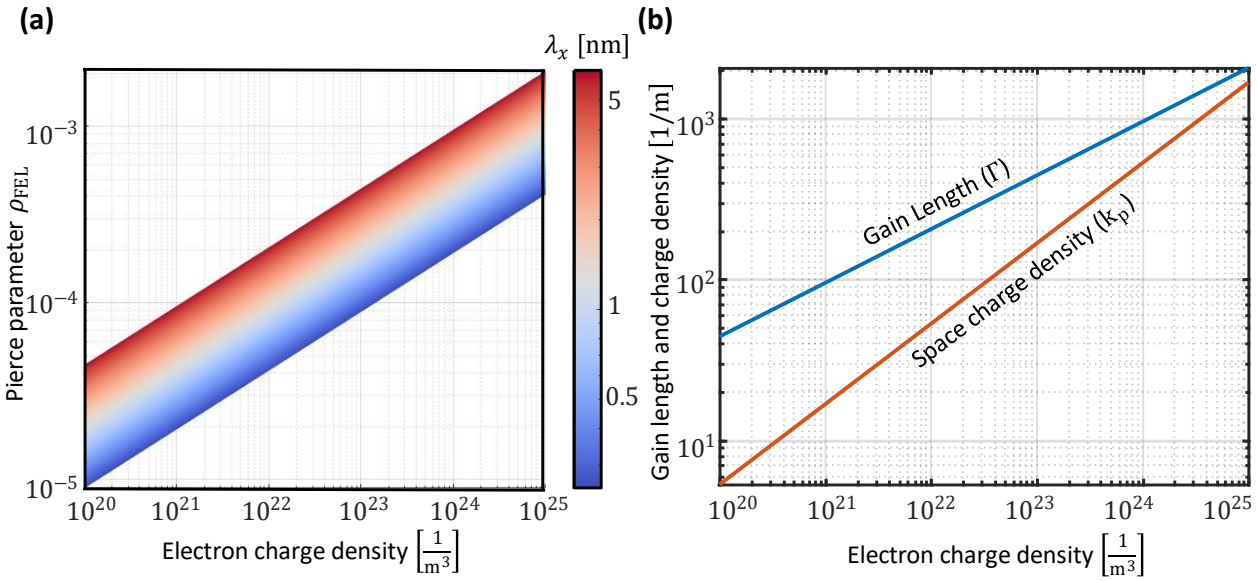

Figure S3: The Pierce parameter and the space charge dependence on the electron charge density. All results were produced for a laser wavelength of $10\mu m$ and $K = 0.1$. **(a)** The Pierce parameter as a function of the electron charge density for different X-ray wavelengths. For longer emission wavelength and denser electron beam charge, the Pierce parameter is higher, easing the requirements on the electron beam and the laser beam. **(b)** The space charge density (k_p) and the gain length (Γ) as a function of the electron charge density for $\lambda_x = 1\ nm$. To avoid the repulsive forces between the electrons, the space charge density should be smaller than the gain length (i.e., $k_p \ll \Gamma$). For denser electron charge pulse, the space charge density parameter increases more rapidly than the gain length. Therefore, the space charge sets an upper limit on the possible electron charge density that can be used in the electron micro-bunching process.

Space charge

The electron repulsive force opposes the bunching ponderomotive force. Therefore, a design criterion is for the FEL gain parameter to be larger than the repulsive forces. The space charge length accounts for the repulsion between the electrons in a bunch and is given by:

$$k_p = \sqrt{\frac{2k_u\mu_0 n_e e^2 c}{\gamma_e m_e \omega_x}} = \frac{1}{\gamma_e}\sqrt{\frac{n_e e^2}{\gamma_e \epsilon_0 m_e c^2}} \qquad \text{(S24)}$$

,

Thus, an important design criterion is that the FEL gain parameter will be larger than the space charge length., i.e., $k_p \ll \Gamma$. Figure S3(b) compares the gain parameter and the space charge as a function of the electron charge density. The space charge parameter (k_p) scales more rapidly than the FEL gain parameter (Γ) as a function of the electron charge density due to the $k_p \propto \sqrt{n_\mathrm{e}}$ and $\Gamma \propto n_\mathrm{e}^{1/3}$ dependence. Therefore, for large electron charge densities (or shorter X-ray wavelengths), the space charge parameter becomes more crucial for the micro-bunching process. Higher electric fields (i.e., more intense laser pulses) can partially overcome this limitation due to the $\Gamma \propto K^{2/3}$ dependence. It is important to note that this parameter is less critical for electron micro-bunching compared with the electron beam energy spread [6].

3.5 The FEL requirements

We analyze below the requirements for the electron micro-bunching and coherent X-ray emission process. The requirements include the electron beam emittance, the electron beam energy spread, the interaction length, the X-ray diffraction condition, the quantum recoil, and electron pulse density and space charge [6]. The laser system requirements will be discussed in the next section.

The electron beam emittance

The electron beam emittance is the most demanding parameter which influences the FEL mechanism due to several reasons: 1) it is responsible for the effective energy spread of the electron beam (Figure 3(a) in the main text). 2) it sets a lower limit to the X-ray wavelength in a fully coherent scheme. In more detail, it affects the following parameters:

1. X-ray energy spread due to electron beam divergence – as described in Eq. (S5), the emitted X-ray energy spread is determined by the electron source divergence. To maintain the conditions of ICS in high-gain regime, it is required that [4]:

$$\gamma_\mathrm{e}^2 \sigma_{x'}^2 = \gamma_\mathrm{e}^2 \theta^2 \leq \frac{1}{2}\rho_\mathrm{FEL}, \tag{S25}$$

   This requirement on the electron beam divergence also limits the minimal electron beam spot size:

$$\sigma_x^2 = \frac{\epsilon_n^2}{(\gamma_\mathrm{e}\theta)^2} \geq \frac{2\epsilon_n^2}{\rho_\mathrm{FEL}}, \tag{S26}$$

2. Electron pulse density - to maintain a quasi-constant electron pulse density during the interaction period, we demand the beam divergence multiplied by the interaction length will be smaller than the beam spot size:

$$\sigma_{x'} L_\mathrm{sat}/2 \leq \sigma_x \tag{S27}$$

This requirement is analogous to the electron beam beta function definition:

$$\sigma_x^2(z) = \epsilon_x \beta_x(z) \rightarrow \sigma_x = \sigma_{x'} \beta_x(z) \rightarrow \beta_x(z) \geq L_{\mathrm{sat}}$$

Therefore, the average electron beam beta function should satisfy:

$$\beta_{\mathrm{av}} \geq L_{\mathrm{sat}}/2 \tag{S28}$$

An additional parameter it affects is the X-ray diffraction condition, as discussed in section 3.5.

The electron beam energy spread

The energy spread, including the effective term, should be smaller than the Pierce parameter:

$$\frac{\sigma_E}{E} = \sqrt{\left(2\frac{\Delta\gamma_{\mathrm{e}}}{\gamma_{\mathrm{e}}}\right)^2 + \left(\frac{\epsilon_{xn}^2}{\sigma_x^2}\right)^2} \leq \frac{1}{2}\rho_{\mathrm{FEL}}, \tag{S29}$$

where σ_E is the energy spread which accounts all the terms in Eq. (S5) - (S6). Typically, the Pierce parameter is $10^{-4} - 10^{-3}$ for the FEL case, but $10^{-5} - 10^{-4}$ for the ICS case, therefore the electron beam energy spread should be an order lower than in FEL facilities.

Laser pulse duration and interaction length

Undulator length should be larger than the gain length:

$$N_u \lambda_u > L_G, \tag{S30}$$

where N_u is the number of laser periods and L_G is the FEL gain length. This requirement suggests that the laser pulse duration should be long enough (~tens of picosecond for soft X-ray to hundreds of picoseconds for hard X-ray).

X-ray diffraction condition

The FEL gain length should be shorter than the radiation Rayleigh range (radiation of the X-ray beam):

$$L_{g0}\,/Z_R^{(X)} < 1/2\,, \tag{S31}$$

where $Z_R^{(X)}$ is the Rayleigh length of the X-ray beam, given by $Z_R^{(X)} = \frac{\pi w_0^2}{\lambda_x}$. This requirement suggests that the X-ray beam will not broaden too much within a period of FEL gain length. Since the X-ray beam Rayleigh length should be larger than the FEL gain length, a larger beam spot size

is preferable, i.e., $\sigma_x^2 = \frac{Z_R^{(X)}\lambda_x}{4\pi} \geq \frac{L_{g0}\lambda_x}{8\pi}$, putting an additional requirement on the minimal electron beam size.

As discussed in Section 2.5 of the main text, the X-ray diffraction condition is equivalent to the requirement that the opening angle of the superradiant cone is smaller than the opening angle of spontaneous ICS emission. We now show this equivalence.

For a fully transversely coherent beam, the opening angle of the superradiant cone satisfies the condition:

$$\sigma_{\mathrm{e}}\Theta_{\mathrm{SR}} = \frac{\lambda_x}{4\pi}$$

where $\sigma_{\mathrm{e}} = \sigma_{\perp}$ is the electron beam spot size. This condition is equivalent to Eq. (S16). In addition, the opening angle of the spontaneous ICS emission is given by $\Theta_1 = \gamma_{\mathrm{e}}^{-1}\sqrt{\rho_{\mathrm{FEL}}}$. Thus, to ensure $\Theta_1 \leq \Theta_{\mathrm{SR}}$, we require:

$$\Theta_1 = \gamma_{\mathrm{e}}^{-1}\sqrt{\rho_{\mathrm{FEL}}} \leq \Theta_{\mathrm{SR}} = \frac{\lambda_x}{4\pi}\frac{1}{\sigma_{\mathrm{e}}}, \tag{S32}$$

where the Pierce parameter ρ_{FEL} is related to the gain length L_{g0} as (Eq. (S23)):

$$L_{g0} = \frac{1}{\sqrt{3}\Gamma} = \frac{\lambda_u}{4\pi\sqrt{3}\rho_{\mathrm{FEL}}},$$

Substituting this relation into Eq. (S33) leads to,

$$\gamma_{\mathrm{e}}^{-1}\sqrt{\rho_{\mathrm{FEL}}} = \gamma_{\mathrm{e}}^{-1}\sqrt{\frac{2\lambda_x\gamma_{\mathrm{e}}^2}{4\pi\sqrt{3}L_{g0}}} \leq \frac{\lambda_x}{4\pi}\frac{1}{\sigma_{\mathrm{e}}}.$$

Rearranging terms leads to,

$$\frac{1}{\sqrt{3}L_{g0}} \leq \frac{\lambda_x}{4\pi}\frac{1}{\sigma_{\mathrm{e}}^2} \rightarrow \sigma_{\mathrm{e}}^2 \leq \frac{\lambda_x}{8\pi}\sqrt{3}L_{g0},$$

which is aligns with the condition outlined in Eq. (S31).

Quantum recoil

For short undulation length or very short X-ray emission, quantum recoil effects become important. From energy conservation considerations, when emitting an X-ray photon, the electron loses the same amount of energy as the photon energy. When the emitted photon energy is in the same order (or larger) than the allowed electron energy spread (defined by Pierce parameter), then the electron beam statistics changes and the effective energy spread may become larger than allowed. Therefore, the quantum recoil parameters defined by:

$$q = \frac{\hbar\omega_x}{\rho_{\mathrm{FEL}}\gamma_{\mathrm{e}}m_{\mathrm{e}}c^2}, \tag{S33}$$

defines the allowed relative photon energy to the electron energy loss. The case where quantum recoil become dominant is $q > 1$.

The requirement for the quantum recoil sets a limit on the upper emitted X-ray energy. The quantum recoil effect is much more significant in the high-gain ICS compared with the undulator FEL, since the electron energy is ~three orders higher in the undulator FEL compared with the high-gain ICS. For the case of $q\sim1$, the quantum recoil effect requires slightly higher beam powers [8]. We will mainly focus on this work in the regime where the quantum recoil is negligible, i.e., $q \leq 1$.

Electron pulse density and space charge

Higher electron pulse density is preferable due to the dependence of the FEL length on the charge density ($L_{g0} \propto n_{\mathrm{e}}^{-1/3}$). However, the electron pulse density is limited by several factors: the conditions on the minimal electron beam size and due to the repulsive force of the bunched electron pulse. In particular, the space charge density should be smaller than the FEL gain length:

$$k_p \ll \Gamma, \tag{S34}$$

This requirement suggests that the electron repulsion forces will be weaker than the bunching ponderomotive force. In section 5.1, we find the limit on the electron pulse density due to this requirement.

4. The counter-propagating laser beam

4.1 Overview

In the previous section, we considered the conditions for electron micro-bunching, assuming an ideal laser system (i.e., strong electric field, large beam spot size, long Rayleigh length, and negligible fluctuations). In this section, we analyze the requirements the laser beam should meet to satisfy the micro-bunching process. The ideal laser beam should have a constant electric field (both the amplitude and the phase terms), with no dependence on the transverse or longitudinal dimension, all along the interaction length in order to avoid broadening of the X-ray linewidth. It is an essential requirement since the electrons' undulation motion (and thus also the X-ray linewidth) depends on the electric field applied to the electron beam (Eq. (S7)). Therefore, to preserve the coherence of the X-ray emission during the interaction, a constant electric field is necessary, resulting the following requirements on the laser system: 1) a large electric field E_0 for an effective interaction with the electron beam; 2) the laser beam spot size ($w_0^{(L)}$) should be much larger than the electron beam spot size in order to maintain a quasi-constant electric field in the

transversal dimension; 3) the counter-propagating laser Rayleigh length ($z_R^{(L)}$) should be longer than the interaction length in order to maintain a quasi-constant electric field in the longitudinal dimension; 4) the laser pulse duration ($\tau_p^{(L)}$) should be long enough to satisfy the requirement for the necessary interaction length and for the X-ray linewidth broadening due to the laser linewidth to be lower than the Pierce parameter. Of course, under the power and energy constraints of the laser pulse, the above requirements compete, and a trade-off between them exists, which we will analyze in this section.

The assumptions about the laser beam are: 1) a single-mode structure of TEM00. 2) The coherence length of the laser system is optimized for the transform-limited pulse duration. 3) The laser beam fluctuations within a pulse satisfy the condition given by Eq. (S7) (Figure 3(c) in the main text). 4) The laser beam Rayleigh length is much longer than the interaction length (Figure 3(b) in the main text).

Table S3 summarizes the parameters that we will use throughout this section. For simplicity, in this section we will remove the L symbol notation which describes the counter-propagating laser beam. We will assume through the discussion that the laser is in a single-mode configuration; thus, its electric field is given by [9]:

$$\boldsymbol{E}(\rho,z) = E_0\hat{\boldsymbol{x}}\frac{w_0}{w(z)}\exp\left(-\frac{\rho^2}{w^2(z)}\right)\exp\left(-i\left(kz+\frac{k\rho^2}{2R(z)}-\psi(z)\right)\right) \tag{S35}$$

where ρ is the radial distance from the center axis of the beam, z is the axial distance from the beam's waist, w_0 is the beam waist, $w(z)$ is the radius at which the amplitude falls to 1/e of the axial value, $R(z)$ is the radius of curvature of the beam's wavefront at z, and $\psi(z)$ is the Gouy phase. These parameters are given by [9]:

$$\begin{aligned} w(z) &= w_0\sqrt{1+\left(\frac{z}{z_R}\right)^2} \\ R(z) &= z\left[1+\left(\frac{z_R}{z}\right)^2\right] \\ \psi(z) &= \arctan\left(\frac{z}{z_R}\right) \end{aligned} \tag{S36}$$

In the following sections we will analyze each one of the requirements in detail, i.e., the laser phase, intensity, duration, beam spot size and Rayleigh length).

#	Parameter	Description
1	w_0	Beam waist. It should be much larger than the electron beam spot size.
2	z_R	Rayleigh length. It should be much longer than the FEL gain length for constant electric field in the longitude dimension.
3	τ_p	The laser pulse duration. It should be long enough for the interaction length and for low laser linewidth.
4	$w(z)$	The radius at which the amplitude falls to 1/e of the axial value
5	$R(z)$	Radius of curvature of the beam's wavefront at z
6	$\psi(z)$	Gouy phase

Table S3: Parameters of the counter-propagating laser beam.

4.2 The electric field phase

First, we will treat the electric field phase term. The phase term should maintain coherence along the longitude interaction length for the validity of the slowly varying amplitude and phase approximation to hold (i.e., the phase term should be as sinusoidal as possible with no dependence on the transversal distance from the z axis). Under the approximation of long Rayleigh length compared with the interaction length ($L_{\text{sat}} \ll z_R$) and large laser beam waist compared with the electron beam size ($r_b \ll w_0$), we can approximate the above quantities as follows:

$$\begin{aligned} w(z) &\approx w_0\left[1+\frac{1}{2}\left(\frac{z}{z_R}\right)^2\right] \\ R(z) &\approx \frac{z_R^2}{z} \\ \psi(z) &\approx \frac{z}{z_R} \end{aligned} \tag{S37}$$

Substituting Eq. (S37) into Eq. (S35), the following phase term is derived:

$$kz+\frac{k\rho^2}{2R(z)}-\psi(z) \approx kz+\frac{k\rho^2}{2z_R^2}z-\frac{z}{z_R}=kz\left(1+\frac{\rho^2}{2z_R^2}-\frac{1}{kz_R}\right) \tag{S38}$$

If the two terms $\frac{\rho^2}{2z_R^2}$ and $\frac{1}{kz_R}$ would satisfy $\frac{\rho^2}{2z_R^2}, \frac{1}{kz_R} \ll \rho_{\text{FEL}}$, then the phase term could be approximated to:

$$kz\left(1+\frac{\rho^2}{2z_R^2}-\frac{1}{kz_R}\right) \approx kz \tag{S39}$$

The term $\frac{\rho^2}{2z_R^2}$ is typically much smaller than the Pierce parameter (i.e., $\frac{r_b^2}{2z_R^2} \ll \rho_{\text{FEL}}$, where r_b is the electron radius). For example, for an electron beam radius of $r_b = 5\mu\text{m}$ and laser Rayleigh length of $z_R = 10\text{cm}$, this term is 4-5 orders of magnitude lower than the Pierce parameter ($\frac{\rho^2}{2z_R^2} \approx$

$10^{-9} \ll \rho_{\mathrm{FEL}}$). The second term $\frac{1}{kz_R}$ is also smaller than the Pierce parameter. First, we derive the value of kL_{sat}:

$$kL_{\mathrm{sat}} \approx \frac{2\pi}{\lambda_L}\frac{\lambda_u}{\rho_{\mathrm{FEL}}} = \frac{\pi}{\rho_{\mathrm{FEL}}}, \tag{S40}$$

Since, $\frac{1}{kz_R} \ll \frac{1}{kL_{\mathrm{sat}}}$, we get that $\frac{1}{kz_R} \ll \rho_{\mathrm{FEL}}$, as required. Therefore, under the assumption above, the electric field is simplified to the form:

$$\boldsymbol{E}(\rho, z) \approx \hat{\boldsymbol{x}} E_0 \frac{w_0}{w(z)} \exp\left(-\frac{\rho^2}{w^2(z)}\right) \exp(-ikz) \tag{S41}$$

4.3 Laser beam intensity fluctuation

From (Eq. (S3)), the X-ray linewidth is determined (among other parameters) from the laser fluctuation. For the case of the linear ICS regime ($K \ll 1$), the requirement can be simplified to:

$$\left(\frac{\Delta\lambda_x}{\lambda_x}\right)_{\text{laser fluctuations}} \approx K^2 \frac{\Delta K}{K} = K^2 \frac{\Delta E_0}{E_0} \tag{S42}$$

This term should be much smaller than the Pierce parameter. Eq. (S42) can be rearranged in terms of the laser intensity as follows:

$$K^2 \frac{\Delta E_0}{E_0} = \frac{1}{2} K^2 \frac{\Delta I_0}{I_0}$$

Therefore, the following requirement on the undulator parameters should be met:

$$K^2 \ll 2\rho_{\mathrm{FEL}} \left(\frac{\Delta I_0}{I_0}\right)^{-1} \tag{S43}$$

Or, equivalently, the following requirement on the laser intensity noise fluctuations:

$$\left(\frac{\Delta I_0}{I_0}\right) \leq \frac{\rho_{\mathrm{FEL}}}{K^2} \tag{S44}$$

where I_0 is the laser average intensity and ΔI_0 is the rms of the laser beam intensity fluctuation. One should note that while the LHS in Eq. (S43) scales as $K^2 \propto I_0$, the RHS scales as $\rho_{\mathrm{FEL}} \propto I_0^{1/3}$. Therefore, this requirement limits the maximal allowed laser pulse intensity. For typical values of $\lambda_L = 1\mu\mathrm{m}$, $K \approx 0.05$ and $\rho_{\mathrm{FEL}} \approx 5 \times 10^{-5}$, it implies that the electric field fluctuation should be $\frac{\Delta E_0}{E_0} \ll 0.02$ or $\frac{\Delta I}{I_0} \ll 0.04$, i.e., the laser intensity fluctuation should be below 1%. The laser fluctuations can rise due to instabilities in the production of the beam or due to the beam divergence after the Rayleigh length (Figure 3(b) and Figure 3(c) in the main text). We will assume the laser

source intensity noise is below the threshold specified by Eq. (S44), and we analyze the electric field change due to the beam divergence. We simplify the electric field amplitude term in Eq. (S41):

$$E_0 \frac{w_0}{w(z)} \exp\left(-\frac{\rho^2}{w^2(z)}\right) \approx E_0 w_0 \left[1 - \frac{1}{2}\left(\frac{z}{z_R}\right)^2\right]\left[1 - \frac{\rho^2}{w^2(z)}\right]$$

From Eq. (S42), the following two conditions should be satisfied:

$$\begin{aligned} K^2 \frac{r_b^2}{w_0^2} &\leq \frac{1}{2}\rho_{\mathrm{FEL}} \\ \frac{K^2}{8}\left(\frac{L_{\mathrm{sat}}}{z_R}\right)^2 &\leq \frac{1}{2}\rho_{\mathrm{FEL}}, \end{aligned} \tag{S45}$$

where we used $\rho \leq r_b$ and $z \leq \frac{L_{\mathrm{sat}}}{2}$ (Figure 4(b) in the main text). The second term in Eq. (S45) is a stricter requirement compared with the first term. For example, if we take an electron beam radius of $r_b = 5$ μm, and laser beam spot waist of $w_0 = 200$ μm, then $K^2 \frac{r_b^2}{w_0^2} \ll 10^{-5}$, fulfilling the first requirement in Eq. (S45). Thus, the overall laser electric field can be approximated by:

$$\boldsymbol{E}(z) \approx \hat{\boldsymbol{x}} E_0 \left[1 - \frac{1}{2}\left(\frac{z}{z_R}\right)^2\right] \exp(-ikz) \tag{S46}$$

If the electric field fluctuation in Eq. (S45) is small enough, such that the condition of Eq. (S43) is satisfied, the assumption on the coherent high-gain ICS scheme will be similar to the external field applied by an undulator magnet. Thus, the high-gain ICS scheme conditions will be identical to those of an undulator FEL. We will discuss in the next section the requirements for the laser Rayleigh length and the beam waist.

4.4 Electric field amplitude

Figure S4 shows the dependence of the electric field on the requirements of Eq. (S43). As the electric field increases, this requirement is harder to satisfy due to the $K^2 \propto E_0^2$ and $\rho_{FEL} \propto E_0^{2/3}$ dependence. Increasing the electron charge density or using longer X-ray wavelengths can relax the requirement.

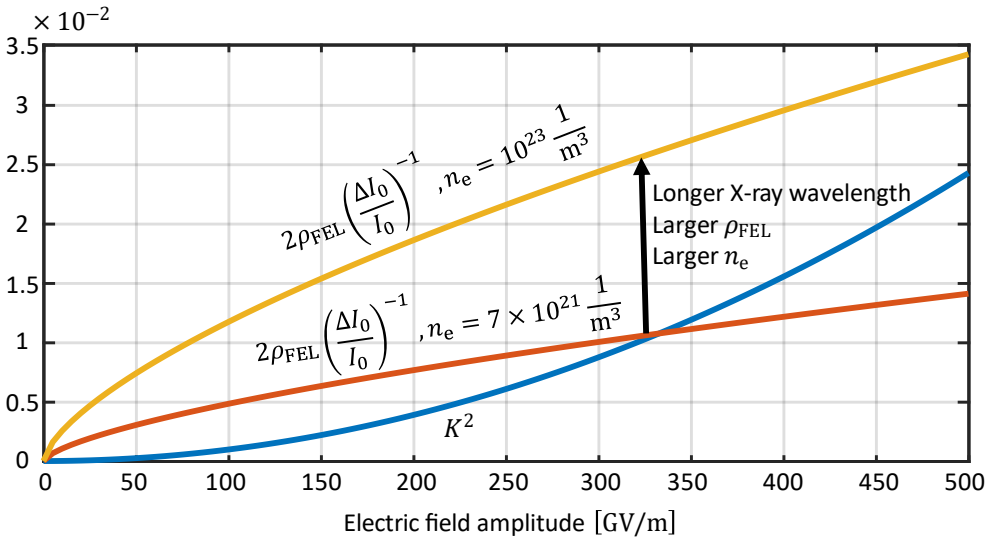

Figure S4: Limitation on the laser beam fluctuations as a function of the electric field strength. The parameters that were used to generate the graph: X-ray wavelength $\lambda_x = 1\text{nm}$, $\lambda_L = 1\mu\text{m}$, $(\Delta I_0/I_0) = 1\%$. The blue line is K^2, the orange line is $2\rho_{\text{FEL}}(\Delta I_0/I_0)^{-1}$, with electron charge density of $n_e = 7\times10^{21}\frac{1}{\text{m}^3}$ and the yellow line is $2\rho_{\text{FEL}}(\Delta I_0/I_0)^{-1}$ with $n_e = 10^{23}\frac{1}{\text{m}^3}$. The requirement $K^2 \ll 2\rho_{\text{FEL}}(\Delta I_0/I_0)^{-1}$ should be satisfied. As the electric field increases, this requirement is harder to satisfy due to $K^2 \propto E_0^2$ and $\rho_{\text{FEL}} \propto E_0^{2/3}$ dependence. The requirement can be relaxed by increasing the Pierce parameter, either by increasing the electron charge density or using longer X-ray wavelengths.

4.5 Laser beam waist and Rayleigh length

In this section, we find the requirements on the laser Rayleigh length and beam waist, following the condition of Eq. (S45). The X-ray linewidth broadening due to the counter-propagating laser beam is the RMS sum of the laser pulse intensity fluctuation over time, and the laser divergence. If the laser beam fluctuations were in the regime for which $K^2\frac{\Delta E_0}{E_0} \ll \rho_{\text{FEL}}$, we could use a high undulator parameter (i.e., a high-intensity laser). However, since $\frac{\Delta K}{K} \gg \rho_{\text{FEL}}$, the allowed maximal laser intensity is limited. From Eq. (S45), the Rayleigh length should satisfy:

$$z_R \geq \frac{KL_{\text{sat}}}{2\sqrt{\rho_{\text{FEL}}}} \approx \frac{K\lambda_L}{4\rho_{\text{FEL}}^{3/2}}, \tag{S47}$$

Due to the relation between the Rayleigh length and the beam waist $z_R = \pi w_0^2/\lambda_L$, we get the following lower bound to the beam waist:

$$w_0 = \sqrt{\frac{z_R\lambda_L}{\pi}} \geq \frac{\lambda_L}{2}\sqrt{\frac{K}{\pi\rho_{\text{FEL}}^{3/2}}}, \tag{S48}$$

Substituting the direct values of the Pierce parameter gives the following bound:

$$w_0 \geq \frac{\sqrt{\lambda_L}}{2}\sqrt{\frac{8\sqrt{2}}{\sqrt{\frac{\pi r_e n_e}{\gamma_e^3}}}} = \sqrt{2\lambda_L}^4\sqrt{\frac{2\gamma_e^3}{\pi r_e n_e}}, \tag{S49}$$

Eq. (S49) shows the relation between the requirements of the laser beam and the electron beam. For higher electron charge densities and lower electron beam energies, the beam waist bound limit would be smaller, relaxing the requirement on the laser pulse power. Figure S5 shows the minimal laser waist as a function of the electron charge density and for different X-ray wavelengths. In addition, shorter counter-propagating laser wavelengths require smaller laser beam waist. Therefore, for a fixed undulator parameter (K), longer laser wavelength will require lower laser pulse power.

For a realistic counter-propagating laser beam that does not satisfy the diffraction limit, the M^2 parameter determines how close the focus is to the diffraction limit. In this case, the Rayleigh length is $z_R = \frac{\pi w_0^2}{M^2\lambda_L}$, and the laser beam waist lower bound is:

$$w_0 = M\sqrt{\frac{z_R\lambda_L}{\pi}} \geq \frac{M\lambda_L}{2}\sqrt{\frac{K}{\pi\rho_{\mathrm{FEL}}^{3/2}}}, \tag{S50}$$

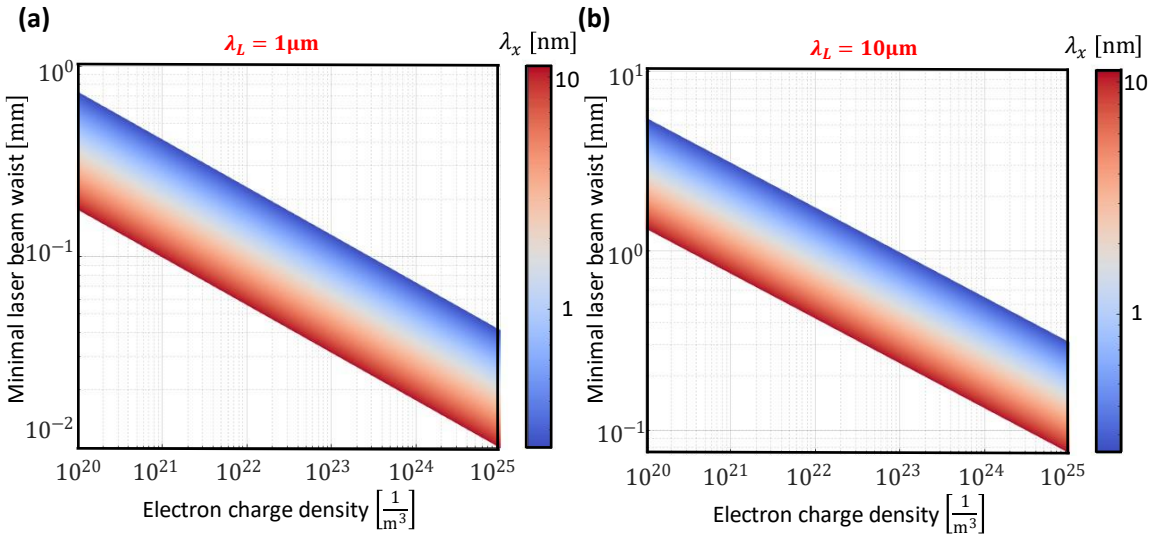

Figure S5: Minimal laser beam waist as a function of the electron charge density for different X-ray wavelengths. The graphs were produced for $K = 0.1$ and laser wavelength of $\lambda_L = 1$ μm (a) and $\lambda_L = 10$ μm (b). The laser beam waist size should be larger for longer laser wavelengths.

4.6 Laser beam power

The laser beam power depends on the required beam intensity and the laser beam waist, by:

$$P_0 = I_0 \pi w_0^2 = \frac{c\epsilon_0 |E_0|^2}{2} \pi w_0^2 \tag{S51}$$

Combing the lower bound of the beam waist (Eq. (S48)) into Eq. (S51) gives the following bound on the laser pulse power:

$$\pi w_0^2 = z_R \lambda_L \geq \frac{K\lambda_L^2}{4\rho_{\mathrm{FEL}}^{3/2}}$$

$$P_0 = I_0 \pi w_0^2 \geq \frac{c\epsilon_0 |E_0|^2}{2} \frac{K\lambda_L^2}{4\rho_{\mathrm{FEL}}^{3/2}} \tag{S52}$$

Explicit values of different configurations will be further shown in section 6.

4.7 Laser pulse duration

The laser pulse duration should be long enough for two reasons: 1) the interaction length should be longer than the interaction length, i.e., greater than $L_{\mathrm{sat}} \approx 20 L_{g0}$. 2) Assuming the laser system is optimized for the Fourier-transform limit of the pulse duration, the laser pulse linewidth should be lower than the Pierce parameter. On the one hand, the Fourier-transform limit of the pulse duration is:

$$\tau_{\mathrm{p}} \Delta\omega_L = 1/2$$

On the other hand, the following should hold:

$$\frac{\Delta\omega_L}{\omega_L} \leq \frac{1}{2}\rho_{\mathrm{FEL}} \rightarrow \Delta\omega_L \leq \frac{1}{2}\omega_L \rho_{\mathrm{FEL}} = \frac{1}{2}\frac{2\pi c}{\lambda_L}\rho_{\mathrm{FEL}}$$

Therefore, combining them gives the lower bound on the pulse duration:

$$\tau_{\mathrm{p}} = \frac{1}{2\Delta\omega_L} \geq \frac{1}{\frac{2\pi c}{\lambda_L}\rho_{\mathrm{FEL}}} = \frac{1}{2\pi}\frac{\lambda_L}{c}\frac{1}{\rho_{\mathrm{FEL}}}$$

$$\tau_{\mathrm{p}} \geq \frac{1}{2\pi}\frac{\lambda_L}{c}\frac{1}{\rho_{\mathrm{FEL}}}, \tag{S53}$$

In addition, the pulse duration should be at least as the required saturation length, i.e.:

$$\tau_{\mathrm{p}} \geq \frac{L_{\mathrm{sat}}}{c} \approx \frac{\lambda_u}{c}\frac{1}{\rho_{\mathrm{FEL}}} = \frac{\lambda_L}{2c}\frac{1}{\rho_{\mathrm{FEL}}}, \tag{S54}$$

Therefore, combining the requirements of Eq. (S53) and Eq. (S54) gives the lower bound for the laser pulse duration.

4.8 Laser pulse energy

Combining the requirements of the laser pulse power and pulse duration, gives the requirement for the total pulse energy of the laser:

$$E_{\mathrm{p}}^{(\mathrm{laser})} = P_0\tau_{\mathrm{p}} \geq \frac{c\epsilon_0|E_0|^2}{2}\frac{K\lambda_L^2}{4\rho_{\mathrm{FEL}}^{3/2}}\frac{\lambda_L}{2c}\frac{1}{\rho_{\mathrm{FEL}}} = \frac{c\epsilon_0|E_0|^2}{2}\frac{K\lambda_L^3}{8c\rho_{\mathrm{FEL}}^{5/2}}$$

$$E_{\mathrm{p}}^{(\mathrm{laser})} \geq \frac{c\epsilon_0|E_0|^2}{2}\frac{K\lambda_L^3}{8c\rho_{\mathrm{FEL}}^{5/2}}, \tag{S55}$$

Figure S6 shows the requirements for the laser pulse duration (τ_{p}) and pulse energy ($\mathrm{E_p}$) as a function of the electron pulse density (n_e) and for different values of electric field amplitude ($\mathrm{E_0}$). Denser electron charge eases the requirements on the laser beam duration and energy. Moreover, while the pulse duration increases for weaker electric field strength, the total electron pulse energy decreases due to the dependence of $E_{\mathrm{p}}^{(\mathrm{laser})} \propto \frac{|E_0|^2K}{\rho_{\mathrm{FEL}}^{5/2}} \propto E_0^{4/3}$. In addition, the laser pulse energy scales as $E_{\mathrm{p}}^{(\mathrm{laser})} \propto \gamma_{\mathrm{e}}^{5/2}\lambda_L^{2/3}$; therefore, either shorter laser wavelength or lower electron energies will ease the requirements on the laser pulse energy. For hard X-rays, these requirements are hard to achieve with current laser technology; thus, we will discuss in section 7 the feasibility of low-gain ICS sources in this spectrum range.

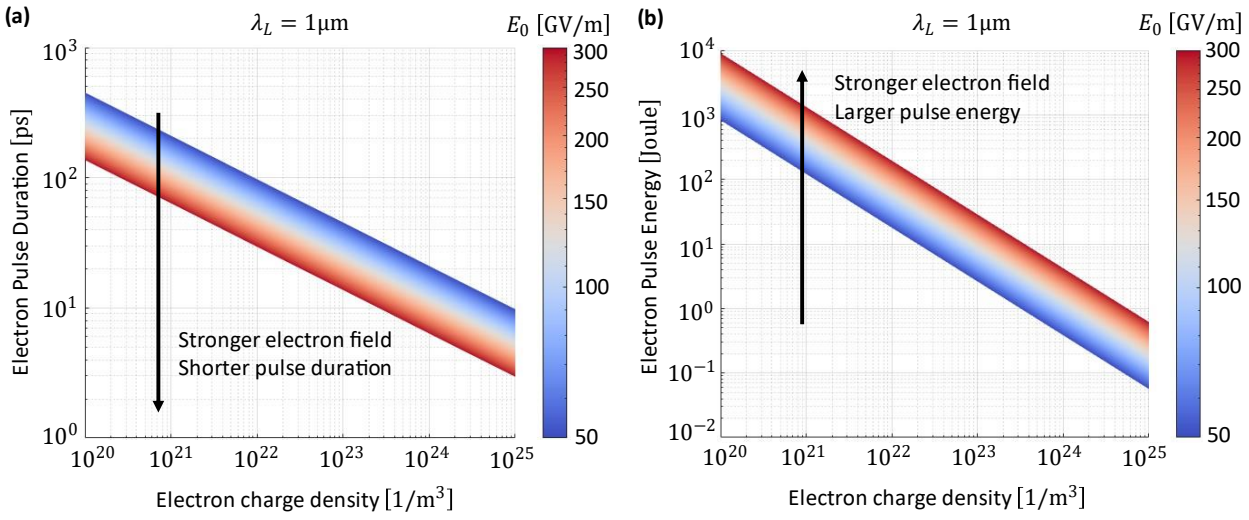

Figure S6: The laser pulse duration (τ_p) and energy (E_p) limits as a function of the electron charge density (n_e) for different electric field amplitudes (E_0). The graphs were produced for $\lambda_L = 1\ \mu m$, $\lambda_x = 1\ nm$.

5. The high-gain inverse Compton scattering bounds

In this section, we analyze the theoretical performance bounds of the coherent high-gain ICS scheme under the quantum mechanical constraints on the electron source brightness. We start from the 6D quantum mechanical bound on the electron brightness and derive the laser beam conditions for the electron micro-bunching. Then, we derive the bound on the power and brightness of the sources under these conditions.

The assumptions made in this section include: 1) the electron source brightness is "ideal", i.e., it achieves the quantum mechanical brightness bound for an electron beam. 2) The electron beam emittance satisfies the condition for a transverse (spatial) coherence emission (Eq. (S16)). 3) The undulator parameter is much smaller than unity ($K \ll 1$, the linear ICS regime), in which $\lambda_x \approx \frac{\lambda_L}{4\gamma_e^2}$. One should note that the second assumption suggests that the electron beam emittance can be sufficiently small or, equivalently, the electron charge density is large enough. This assumption will come at the expense of lower electron pulse charge and peak current.

5.1 Upper bound of the electron charge density

The fundamental limits in beam brightness set by quantum mechanics are at least 4-5 orders of magnitude higher than the performance of state-of-the-art pulsed electron sources [5]. Therefore, it presents an optimistic view of the opportunities for significant improvements and further breakthroughs in the spectrum of bright electron beam applications. By the quantum-mechanical bound, the current density of an electron beam that satisfies $\gamma_\mathrm{e} \gg 1$ and $\Delta\gamma_\mathrm{e} \ll \gamma_\mathrm{e}$ in the absence of external electromagnetic fields is given by [10]:

$$J_\mathrm{e} = e\beta c\frac{N_\mathrm{e}}{V} = e\beta c n_\mathrm{e} \leq \frac{2ec\beta^2\,\gamma_\mathrm{e}^2\,\Delta\gamma_\mathrm{e}\Omega}{\lambda_c^3}, \tag{S56}$$

where N_e is the number of electrons confined into a volume V, $n_\mathrm{e} = N_\mathrm{e}/V$ is the electron charge density, $\Delta\gamma_\mathrm{e}$ is the energy spread, $\lambda_c = \frac{h}{mc} = 2.43\mathrm{pm}$ is the Compton wavelength, and Ω is the electron velocity divergence. Thus, the normalized brightness is limited by:

$$B_{n,\mathrm{e}}^{\mathrm{QM-limit}} = \frac{J_\mathrm{e}}{\Omega\gamma_\mathrm{e}^2} = \frac{I_\mathrm{e}}{\pi^2\epsilon_n^2} = \frac{2ec\beta^2\,\Delta\gamma_\mathrm{e}}{\lambda_c^3}, \tag{S57}$$

where I_e is the beam current, and Ω is the solid-angle divergence of the beam. The electron normalized brightness units used in this work are $\left[\frac{\mathrm{C}}{\mathrm{s\,m^2 rad^2}}\right]$. Rearranging Eq. (S57) gives:

$$B_{n,\mathrm{e}}^{\mathrm{QM-limit}} = \frac{2ec}{\lambda_c^3}\left(\frac{\Delta\gamma_\mathrm{e}}{\gamma_\mathrm{e}}\right)\gamma_\mathrm{e}, \tag{S58}$$

Setting the electron beam emittance to fulfill the fully coherent condition (Eq. (S16)), i.e. $\epsilon_n = \frac{\lambda_x}{4\pi}\gamma_\mathrm{e}$, yields the upper limit to the electron source current:

$$I_{\mathrm{e}} \leq \frac{2\pi^2 ec}{\lambda_c^3}\left(\frac{\lambda_x}{4\pi}\right)^2\left(\frac{\Delta\gamma_{\mathrm{e}}}{\gamma_{\mathrm{e}}}\right)\gamma_{\mathrm{e}}^3, \tag{S59}$$

The first question we address is about the upper bounds of a high-gain ICS scheme with an "ideal" electron source. As we will see, the main limitation is the electron charge density and the repulsion forces. The repulsion force between electrons in a dense charge pulse is stronger than the ponderomotive force, opposing the micro-bunching process. Therefore, we would find the upper limit to the electron charge density such that the pondermotive force will be stronger than the repulsion forces. We will use the following steps: 1) Find the electron charge density n_{e} upper bound by the requirement that the repulsion forces between the electron are weaker than the ponderomotive force. 2) Derive the upper limit of the Pierce parameter by the electron charge density bound. 3) The Pierce parameter will set the maximal electron energy spread, and divergence allowed. 4) Derive the maximal electron source current (Eq. (S59)). 5) Derive the coherent ICS X-ray brightness and power limits in the high-gain regime.

The quantum-mechanical brightness bound sets an upper bound to the electron charge density (Eq. (S59). The electron charge density is given by:

$$n_{\mathrm{e}} = \frac{1}{ec}\frac{I_{\mathrm{e}}}{2\pi\sigma_x\sigma_y}, \tag{S60}$$

where σ_x, σ_y are the RMS beam spot size. Substituting $\sigma_x^2\sigma_{x'}^2 = \epsilon_x^2 = \epsilon_n^2/\gamma_{\mathrm{e}}^2$, while assuming $\sigma_x = \sigma_y$, the following bound is derived:

$$n_{\mathrm{e}} = \frac{1}{ec}\frac{I_{\mathrm{e}}\gamma_{\mathrm{e}}^2}{2\pi\epsilon_n^2/\sigma_{x'}^2} \leq \frac{\pi}{\lambda_c^3}\left(\frac{\Delta\gamma_{\mathrm{e}}}{\gamma_{\mathrm{e}}}\right)\gamma_{\mathrm{e}}^3\sigma_{x'}^2, \tag{S61}$$

From the requirements on the electron beam emittance, which should be lower than the Pierce parameter (Eq. (S6)):

$$\gamma_{\mathrm{e}}^2\sigma_{x'}^2 \leq \frac{1}{2}\rho_{\mathrm{FEL}}, \tag{S62}$$

Substituting $\Delta\gamma_{\mathrm{e}}/\gamma_{\mathrm{e}} \leq \rho_{\mathrm{FEL}}/4$ and Eq. (S62) into Eq. (S61), gives the following requirement on the electron charge density:

$$n_{\mathrm{e}} \leq \frac{\pi}{\lambda_c^3}\gamma_{\mathrm{e}}\frac{1}{8}\rho_{\mathrm{FEL}}^2, \tag{S63}$$

A stricter bound on the electron charge density n_e arises from the requirement that the space charge repulsion forces will be weaker than the ponderomotive force (i.e., the gain length). In other words, we demand $k_p \leq \Gamma$:

$$k_p \leq \Gamma \rightarrow \sqrt{\frac{2k_u\mu_0 n_\mathrm{e} e^2 c}{\gamma_\mathrm{e} m_\mathrm{e}\omega_x}} \leq \frac{4\pi}{\lambda_u}\rho_\mathrm{FEL} \rightarrow \sqrt{\frac{2k_u\mu_0 n_\mathrm{e} e^2 c}{\gamma_\mathrm{e} m_\mathrm{e}\omega_x}} \leq \frac{2\pi}{\lambda_u}\left(\frac{\pi K^2 r_\mathrm{e} n_\mathrm{e}}{k_u^2\gamma_\mathrm{e}^3}\right)^{\frac{1}{3}} \rightarrow$$

$$\rightarrow \left(\frac{2k_u\mu_0 n_\mathrm{e} e^2 c}{\gamma_\mathrm{e} m_\mathrm{e}\omega_x}\right)^3 \leq k_u^6\left(\frac{\pi K^2 r_\mathrm{e} n_\mathrm{e}}{k_u^2\gamma_\mathrm{e}^3}\right)^2$$

Rearranging the term, while substituting $\omega_x = k_x c \approx 2\gamma_\mathrm{e}^2 k_u c = 4\gamma_\mathrm{e}^2 k_L c$ (for the case $K \ll 1$ in Eq. (S3)):

$$n_\mathrm{e} \leq k_u^6\left(\frac{\pi K^2 r_\mathrm{e}}{k_u^2\gamma_\mathrm{e}^3}\right)^2\left(\frac{\gamma_\mathrm{e} m_\mathrm{e}\omega_x}{2k_u\mu_0 e^2 c}\right)^3 =$$

$$= k_u^6\left(\frac{\pi K^2 r_\mathrm{e}}{k_u^2\gamma_\mathrm{e}^3}\right)^2\left(\frac{\gamma_\mathrm{e} m_\mathrm{e} 2\gamma_\mathrm{e}^2 k_u c}{2k_u\mu_0 e^2 c}\right)^3 = k_u^6\gamma_\mathrm{e}^3\left(\frac{\pi K^2 r_\mathrm{e}}{k_u^2}\right)^2\left(\frac{m_\mathrm{e}}{\mu_0 e^2}\right)^3 = \pi^2 k_u^2\gamma_\mathrm{e}^3 K^4 r_\mathrm{e}^2\left(\frac{m_\mathrm{e}}{\mu_0 e^2}\right)^3$$

The electron radius is $r_\mathrm{e} = \frac{1}{4\pi\epsilon_0}\left(\frac{e^2}{m_\mathrm{e}c^2}\right) = \frac{\mu_0 e^2}{4\pi m_\mathrm{e}}$; thus:

$$\pi^2 k_u^2\gamma_\mathrm{e}^3 K^4 r_\mathrm{e}^2\left(\frac{m_\mathrm{e}}{\mu_0 e^2}\right)^3 = \pi^2 k_u^2\gamma_\mathrm{e}^3 K^4 r_\mathrm{e}^2\left(\frac{1}{4\pi r_\mathrm{e}}\right)^3 = \frac{k_u^2\gamma_\mathrm{e}^3 K^4}{64\pi r_\mathrm{e}}$$

Therefore:

$$n_\mathrm{e} \leq \frac{k_u^2\gamma_\mathrm{e}^3 K^4}{64\pi r_\mathrm{e}}, \tag{S64}$$

As expected, the electron pulse charge upper bound is higher for either higher electron beam energies ($\propto \gamma_\mathrm{e}^3$) or stronger laser fields ($\propto K^4$). Overall, the upper bound of the electron charge density is given by:

$$n_\mathrm{e} \leq \min\left(\frac{k_u^2\gamma_\mathrm{e}^3 K^4}{64\pi r_\mathrm{e}}, \frac{\pi}{\lambda_c^3}\gamma_\mathrm{e}\frac{1}{8}\rho_\mathrm{FEL}^2\right) \tag{S65}$$

where the first term comes from the requirement on the repulsive force and the second on the quantum mechanical limitation on the electron beam brightness. The typical bound in the RHS in Eq. (S63) is several orders of magnitude larger than bound given by the requirement of the repulsion force to be smaller than the ponderomotive force (Eq. (S64)). Therefore, the condition in Eq. (S64) sets the bound for the electron charge density, i.e., the repulsion forces are the limiting factor in the high-gain scheme for an "ideal" electron source.

Figure S7 shows the upper bound of the electron charge density as a function of electron energy for $\lambda_L = 1\mu\text{m}$. The typical values are $10^{25} - 10^{26}$ $[1/\text{m}^3]$, 3-4 orders higher than state-of-the-art electron beam sources.

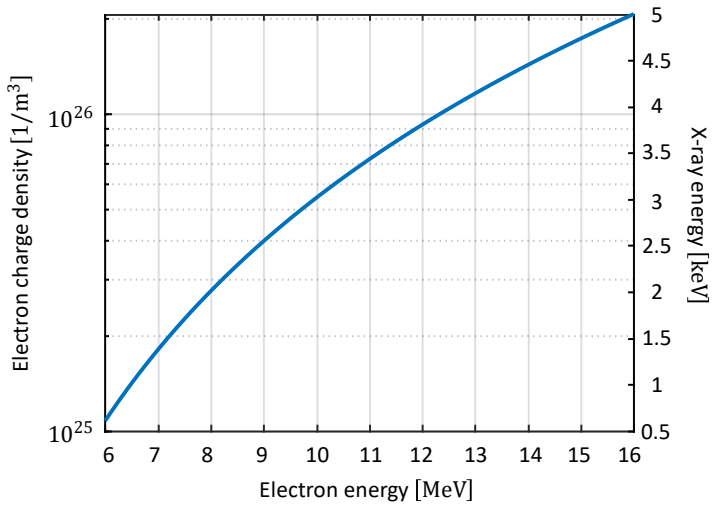

Figure S7: Upper bound for the electron charge density as a function of the electron energy. The graph was produced with $\lambda_L = 1\mu m$ and $K = 0.07$.

5.2 Upper bound of the electron beam current

Substituting Eq. (S64) into Eq. (S20) yields the following bound of the Pierce parameter:

$$\rho_{\text{FEL}} = \frac{1}{2}\left(\frac{\pi K^2 r_e n_e}{k_u^2 \gamma_e^3}\right)^{\frac{1}{3}} \leq \frac{1}{2}\left(\frac{\pi K^2 r_e \left(\frac{k_u^2 \gamma_e^3 K^4}{64\pi r_e}\right)}{k_u^2 \gamma_e^3}\right)^{\frac{1}{3}} = \frac{1}{8}K^2$$

$$\rho_{\text{FEL}} \leq \frac{K^2}{8}, \tag{S66}$$

This result is surprising since the Pierce parameter bound depends only on the counter-propagating laser parameters ($K \propto \lambda_L E_0$)! Since the allowed energy spread is limited by the Pierce parameter, the following requirement holds:

$$\frac{\Delta\gamma_e}{\gamma_e} \leq \frac{1}{4}\rho_{\text{FEL}} = \frac{K^2}{32}, \tag{S67}$$

Substituting Eq. (S67) into Eq. (S59), gives the following bound on the electron beam current:

$$I_e \leq \frac{2\pi^2 ec}{\lambda_c^3}\left(\frac{\lambda_x}{4\pi}\right)^2 \frac{\rho_{\text{FEL}}}{4}\gamma_e^3 \leq \frac{2\pi^2 ec}{\lambda_c^3}\left(\frac{\lambda_x}{4\pi}\right)^2 \frac{K^2}{32}\gamma_e^3, \tag{S68}$$

The next question we address is what undulator parameter value to set for the Pierce parameter. Since $\rho_{\mathrm{FEL}} \leq K^2/8$, we would fix $\rho_{\mathrm{FEL}} = 10^{-3}$ to preserve an X-ray beam linewidth of 0.1%. If we take larger values of ρ_{FEL}, then the undulator parameter, K, would need to increase and would not satisfy the assumption of linear ICS. On the other hand, a smaller Pierce parameter than 10^{-3} would cause quantum recoil effects to become more dominant and would decrease the peak power of the scheme; therefore, the Pierce parameter value of 10^{-3} seems the correct trade-off value.

5.3 Upper bound of the electron source brightness

In this section we find the upper limit for the electron source brightness and current, bounded by the requirement for ponderomotive force to be stronger than repulsion forces (Eq. (S64)). As we show in section 6.2, the relation between the electron charge density and the electron source normalized brightness, assuming the conditions of the high-gain ICS, is given by:

$$B_n = \frac{8ec}{\rho_{\mathrm{FEL}}} n_{\mathrm{e}}$$

Substituting Eq. (S64) into this relation, gives the upper bound for the electron source brightness in the high-gain ICS regime:

$$B_n = \frac{8ec}{\rho_{\mathrm{FEL}}} n_{\mathrm{e}} \leq \frac{8ec}{\rho_{\mathrm{FEL}}} \frac{k_u^2 \gamma_{\mathrm{e}}^3 K^4}{64\pi r_{\mathrm{e}}}$$

Substituting $\rho_{\mathrm{FEL}} = K^2/8$ (Eq. (S66)):

$$B_n \leq \frac{ec}{\pi r_{\mathrm{e}}} k_u^2 \gamma_{\mathrm{e}}^3 K^2 = \frac{8ec}{\pi r_{\mathrm{e}}} k_u^2 \gamma_{\mathrm{e}}^3 \rho_{\mathrm{FEL}} = \frac{2ec}{\pi r_{\mathrm{e}}} k_L^2 \gamma_{\mathrm{e}}^3 \rho_{\mathrm{FEL}}$$

Therefore, we derive the following upper bound for the electron source brightness:

$$B_n \leq \frac{2ec}{\pi r_{\mathrm{e}}} k_L^2 \gamma_{\mathrm{e}}^3 \rho_{\mathrm{FEL}}, \tag{S69}$$

The electron source brightness upper bound as derived in Eq. (S69) is up to 4 orders of magnitude lower than the 6D quantum-mechanical bound (Figure S8). Therefore, even if the electron source approaches the upper bound of the 6D quantum-mechanical brightness, it would be restricted much more severely due to the repulsion forces. The difference between the bounds is smaller for higher X-ray energies since the repulsion forces are less severe for higher energy electron beams.

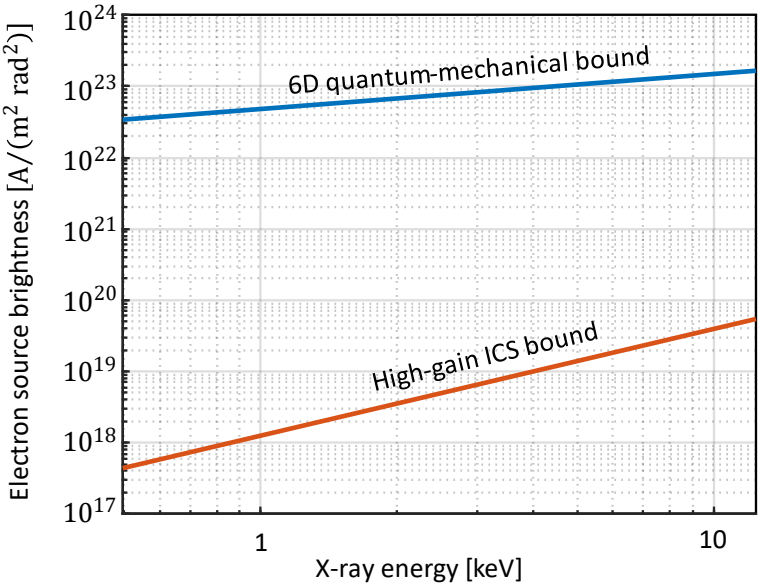

Figure S8: Electron source brightness upper bounds of the 6D quantum-mechanical bound and the high-gain ICS bound (Eq. (S69)) as a function of the X-ray energy. The graph was produced for $\lambda_L = 1\mu m$. The difference between the bounds is smaller for higher X-ray energies.

Next, we find the upper bound for the electron source current, given by the requirement of Eq. (S63):

$$B_n = \frac{I_\mathrm{e}}{\pi^2\epsilon_n^2} \rightarrow I_\mathrm{e} = \pi^2\epsilon_n^2 B_n \rightarrow I_\mathrm{e} \leq \pi^2\epsilon_n^2 \frac{ec}{\pi r_\mathrm{e}} k_u^2 \gamma_\mathrm{e}^3 K^2$$

Rearranging the terms and using the assumption of $K \ll 1$ and $\lambda_x \approx \lambda_L/4\gamma_\mathrm{e}^2$:

$$\pi^2\epsilon_n^2 \frac{ec}{\pi r_\mathrm{e}} k_u^2 \gamma_\mathrm{e}^3 K^2 = \frac{\pi ec}{r_\mathrm{e}} \epsilon^2 \gamma_\mathrm{e}^2 \left(\frac{2\pi}{\lambda_u}\right)^2 \gamma_\mathrm{e}^3 K^2 = \frac{\pi ec}{r_\mathrm{e}} \left(\frac{\lambda_x}{4\pi}\right)^2 \left(\frac{4\pi}{\lambda_L}\right)^2 \gamma_\mathrm{e}^5 K^2$$
$$= \frac{\pi ec}{r_\mathrm{e}} \left(\frac{\lambda_L}{16\pi}\right)^2 \left(\frac{4\pi}{\lambda_L}\right)^2 \gamma_\mathrm{e} K^2 = \frac{\pi ec}{r_\mathrm{e}} \frac{1}{16} \gamma_\mathrm{e} K^2$$

Therefore, we get the upper bound for the electron current:

$$I_\mathrm{e} \leq \frac{\pi ec}{2r_\mathrm{e}} \gamma_\mathrm{e} \rho_\mathrm{FEL} = \frac{\pi ec}{16 r_\mathrm{e}} \gamma_\mathrm{e} K^2, \tag{S70}$$

5.4 Upper bound of the coherent ICS source power and brightness

We derive in this section the upper bounds for the X-ray beam power and brightness, assuming an electron source that achieves the upper bound brightness defined by Eq. (S63). If the conditions for electron micro-bunching are met, a bright X-ray beam is emitted. In undulator FEL facilities, the peak power can reach tens GW and a brightness of $\sim 10^{33}\,\frac{\text{photons}}{\text{s mm}^2\,\text{mrad}^2\,0.1\%\text{BW}}$ [4]. In the coherent high-gain ICS scheme, however, the peak power and the peak brightness will be lower since the total power and energy of the electron beam are much lower. We will derive the scaling law of the peak power and the peak brightness as a function of the electron beam energy and the undulator period. First, the number of photons produced per electron is given by [4]:

$$N_{\text{ph,coherent}}^{\text{single-electron}} = \rho_{\text{FEL}} E_{\text{e}} / E_{\text{ph}} \tag{S71}$$

For the case of $K \ll 1$, the ratio between the electron energy and the emitted X-ray photon energy can be approximated by:

$$\frac{E_{\text{e}}}{E_{\text{ph}}} = \frac{\gamma_{\text{e}} m_{\text{e}} c^2}{\hbar \omega_x} = \frac{\gamma_{\text{e}} m_{\text{e}} c^2}{\hbar \left(\frac{2\pi}{\lambda_x}\right) c} \approx \frac{\gamma_{\text{e}} m_{\text{e}} c}{\hbar \left(\frac{8\pi \gamma_{\text{e}}^2}{\lambda_L}\right)} = \frac{\lambda_L m_{\text{e}} c}{8\pi \hbar \gamma_{\text{e}}} = \frac{1}{4\gamma_{\text{e}}} \frac{\lambda_L}{\lambda_c}$$

$$\frac{E_{\text{e}}}{E_{\text{ph}}} = \frac{1}{4\gamma_{\text{e}}} \frac{\lambda_L}{\lambda_c}, \tag{S72}$$

The Pierce parameter ρ_{FEL} describes the efficiency (or the conversion ratio) between the electron beam power and the X-ray beam saturation power. It is given by the multiplication between the number of photons produced per electron and the electron beam current. Rearranging Eq. (S71) with respect to the Lorentz factor gives:

$$N_{\text{ph,coherent}}^{\text{single-electron}} = \frac{\rho_{\text{FEL}} \gamma_{\text{e}} m_{\text{e}} c^2}{\hbar \omega_x} \approx \frac{\rho_{\text{FEL}} \gamma_{\text{e}} m_{\text{e}} c^2}{\left(\frac{8\pi \hbar c}{\lambda_L}\right) \gamma_{\text{e}}^2} \propto \gamma_{\text{e}}^{-2} \tag{S73}$$

Therefore, Eq. (S73) implies that higher electron beam energies will produce less photons per single electron. Substituting Eq. (S64) and Eq. (S67) into Eq. (S71) gives:

$$P_{\text{sat}} = \rho_{\text{FEL}} P_{\text{e}} = \rho_{\text{FEL}} \gamma_{\text{e}} m_{\text{e}} c^2 \frac{I_{\text{e}}}{e} \leq \rho_{\text{FEL}} \gamma_{\text{e}} m_{\text{e}} c^2 \frac{\pi c}{2 r_{\text{e}}} \gamma_{\text{e}} \rho_{\text{FEL}} = \frac{\pi m_{\text{e}} c^3}{2 r_{\text{e}}} \rho_{\text{FEL}}^2 \gamma_{\text{e}}^2$$

And we get the saturation power bound of the high-gain ICS scheme:

$$P_{\text{sat}}^{\text{QM-limit}} = \frac{\pi m_{\text{e}} c^3}{2 r_{\text{e}}} \rho_{\text{FEL}}^2 \gamma_{\text{e}}^2 \tag{S74}$$

The peak saturation power derived in Eq. (S74) is the upper bound set by the requirement of pondermotive force larger than repulsion forces. The peak power is independent of the electron energy but on the undulation period. Longer undulation period lengths will have greater saturation power. For example, the theoretical peak power bound of the undulator FEL will be ~8-9 orders

of magnitude higher than a coherent ICS scheme with a laser wavelength of 1μm. The quantum-mechanical saturation power bound for a high-gain ICS scheme with $\rho_{\mathrm{FEL}} = 10^{-3}$ and a laser wavelength of 1 μm is ~1GW, similar to state-of-the-art undulator FEL facilities. However, for state-of-the-art electron sources, the coherent ICS saturation power will be much lower, as discussed in the next section.

Next, we derive the bound on the X-ray beam brightness. The X-ray beam brightness is given by:

$$B_{\mathrm{ph}} = \frac{N_{\mathrm{ph}}}{4\pi^2 \epsilon_x \epsilon_y 2\pi \sigma_t \sigma_\omega/\omega}, \tag{S75}$$

where N_{ph} is the total photon emitted, ϵ_x, and ϵ_y are the X-ray beam emittance, σ_t is the RMS of the pulse duration and σ_ω/ω is the X-ray beam linewidth. For the high-gain regime, the X-ray linewidth is [4]:

$$\sigma_\omega/\omega = 3\sqrt{2}\rho_{\mathrm{FEL}}\sqrt{\frac{L_{g0}}{z}}, \tag{S76}$$

For typical interaction length of $z = L_{\mathrm{sat}} \approx 20L_{g0}$, the linewidth is approximately $\sigma_\omega/\omega \approx \rho_{\mathrm{FEL}}$. Since the minimum transverse phase-space volume for a diffraction-limited photon beam is defined, for photons of wavelength λ_x, by $\Delta x \Delta\theta_x \geq \lambda_x/4\pi$ and $\Delta y \Delta\theta_y \geq \lambda_y/4\pi$, substituting Eq. (S16) and Eq. (S76) into Eq. (S75) gives:

$$B_{\mathrm{ph}} = \frac{\rho_{\mathrm{FEL}} E_{\mathrm{e}}}{E_{\mathrm{ph}}} \frac{I_{\mathrm{e}}}{e\, 8\pi^3 \epsilon_x \epsilon_y \sigma_\omega/\omega} = \frac{\rho_{\mathrm{FEL}} E_{\mathrm{e}}}{E_{\mathrm{ph}}} \frac{I_{\mathrm{e}}}{e\, 8\pi^3 (\lambda_x/4\pi)^2 \sigma_\omega/\omega}$$

Then, substituting Eq. (S72) gives:

$$B_{\mathrm{ph}} = \frac{\rho_{\mathrm{FEL}} E_{\mathrm{e}}}{E_{\mathrm{ph}}} \frac{I_{\mathrm{e}}}{e\, 8\pi^3 (\lambda_x/4\pi)^2 \sigma_\omega/\omega} = \frac{1}{4\gamma_{\mathrm{e}}} \frac{\lambda_L}{\lambda_c} \frac{I_{\mathrm{e}}}{e\, 8\pi^3 (\lambda_x/4\pi)^2}$$

Substituting the upper bound for the electron source current leads to (Eq. (S70)):

$$B_{\mathrm{ph}} \leq \frac{1}{4\gamma_{\mathrm{e}}} \frac{\lambda_L}{\lambda_c} \frac{\left(\frac{\pi e c}{2r_{\mathrm{e}}} \gamma_{\mathrm{e}} \rho_{\mathrm{FEL}}\right)}{e\, 8\pi^3 \left(\frac{\lambda_x}{4\pi}\right)^2} = \frac{1}{4} \frac{\lambda_L}{\lambda_c} \frac{\left(\frac{\pi c}{2r_{\mathrm{e}}} \rho_{\mathrm{FEL}}\right)}{8\pi^3 \left(\frac{\lambda_x}{4\pi}\right)^2} = \frac{1}{4} \frac{\lambda_L}{\lambda_c} \frac{\left(\frac{c}{r_{\mathrm{e}}} \rho_{\mathrm{FEL}}\right)}{{\lambda_x}^2} = \frac{1}{4} \frac{\lambda_L}{\lambda_c} \frac{c}{r_{\mathrm{e}}} \frac{\rho_{\mathrm{FEL}}}{{\lambda_x}^2} \approx \frac{1}{4} \frac{\lambda_L}{\lambda_c} \frac{c}{r_{\mathrm{e}}} \frac{\rho_{\mathrm{FEL}}}{\left(\frac{\lambda_L}{4\gamma_{\mathrm{e}}^2}\right)^2}$$

And finally, we derive the upper bound of the high-gain ICS peak brightness:

$$B^{(\mathrm{peak})}_{\mathrm{coherent\ ICS}} = \frac{4c}{\lambda_c r_{\mathrm{e}}} \frac{\rho_{\mathrm{FEL}}}{\lambda_L} \gamma_{\mathrm{e}}^4, \tag{S77}$$

Figure 4(a) in the main text shows the peak brightness for the high-gain ICS with laser wavelengths of $\lambda_L = 1\ \mu$m and $\lambda_L = 10\ \mu$m. The peak brightness scaling laws prefer longer laser wavelengths, i.e., higher electron beam energies and longer wavelengths are advantageous for the source

brightness. However, longer laser wavelengths require more laser pulse energy (Eq. (S55)). Therefore, there is a trade-off between the X-ray beam brightness and the requirements of the counter-propagating laser beam. The brightness of state-of-the-art X-ray FEL facilities is $10^{33}\,\frac{\text{photons}}{\text{s mm}^2\,\text{mrad}^2\,0.1\%\text{BW}}$, comparable to the quantum-mechanical bound of the high-gain ICS scheme.

5.5 Comparison with the incoherent ICS scheme

Next, we compare the coherent high-gain ICS and the incoherent ICS schemes. In the incoherent ICS scheme, we assume the interaction length is L_{g0} (i.e., the low-gain regime), yet the laser pulse power and intensity are the same between the two schemes. The incoherent scheme has a broad emission cone (section 2.3) with an opening angle of $\sim 0.1\gamma_{\mathrm{e}}^{-1}$. Moreover, the shorter interaction length leads to an energy linewidth broadening by an order of magnitude higher than the coherent high-gain regime. From Eq. (S2), assuming $\sigma_L^2 \gg \sigma_{\mathrm{e}}^2$, the total number of emitted X-ray photons in the incoherent ICS scheme is:

$$N_x = \frac{N_{\mathrm{e}} N_L \sigma_T}{2\pi\sigma_L^2} = N_{\mathrm{e}} \frac{N_L}{\sigma_L^2}\frac{\sigma_T}{2\pi}$$

Assuming the laser pulse duration is in the low-gain regime. i.e., $\tau_p = L_{g0}/c$, the counter-propagating laser beam flux is derived:

$$\frac{N_L}{\sigma_L^2} = \frac{I_0^{(\text{laser})}\tau_p}{\hbar\left(\frac{2\pi}{\lambda_L}\right)c} = \frac{\frac{c\epsilon_0|E_0|^2}{2}\tau_p}{\frac{2\pi\hbar c}{\lambda_L}} = \frac{\frac{c\epsilon_0|E_0|^2}{2}}{\frac{2\pi\hbar c}{\lambda_L}}\frac{L_{g0}}{c} = \frac{\frac{c\epsilon_0|E_0|^2}{2}}{\frac{2\pi\hbar c}{\lambda_L}}\frac{\lambda_L}{8\pi\sqrt{3}\rho_{\mathrm{FEL}}c} = \frac{\epsilon_0|E_0|^2}{32\pi^2\sqrt{3}\hbar c}\frac{\lambda_L^2}{\rho_{\mathrm{FEL}}}$$

We set the Pierce parameter bound for an "ideal" electron source, $\rho_{\mathrm{FEL}} = K^2/8$, and get:

$$\frac{N_L}{\sigma_L^2} = \frac{\epsilon_0|E_0|^2}{32\pi^2\sqrt{3}\hbar c}\frac{\lambda_L^2}{\rho_{\mathrm{FEL}}} = \frac{\epsilon_0|E_0|^2}{4\pi^2\sqrt{3}\hbar c}\frac{\lambda_L^2}{K^2} = \frac{\epsilon_0|E_0|^2}{4\pi^2\sqrt{3}\hbar c}\frac{\lambda_L^2}{\left(\frac{eE_0\lambda_L}{2\pi m_{\mathrm{e}}c^2}\right)^2} = \frac{\epsilon_0}{4\pi^2\sqrt{3}\hbar c}\left(\frac{2\pi m_{\mathrm{e}}c^2}{e}\right)^2$$

$$= \frac{1}{2\sqrt{3}}\left(\frac{m_{\mathrm{e}}c}{2\pi\hbar}\right)\left(4\pi\epsilon_0\frac{m_{\mathrm{e}}c^2}{e^2}\right) = \frac{1}{2\sqrt{3}}\frac{1}{\lambda_c r_{\mathrm{e}}}$$

Therefore, for the incoherent ICS scheme, when assuming the laser pulse duration is L_{g0}/c (the low-gain ICS regime), with the same laser power and intensity as the coherent ICS, and an ideal electron source, the number of X-ray photons produced per a single electron is:

$$N_{\mathrm{ph,incoh}}^{\mathrm{single-electron}} = \frac{1}{2\sqrt{3}}\frac{1}{\lambda_c r_{\mathrm{e}}}\frac{\sigma_T}{2\pi} = \frac{2}{3\sqrt{3}}\frac{r_{\mathrm{e}}}{\lambda_c} \approx 5\times10^{-4}, \tag{S78}$$

Comparing the number of emitted photons per electron between the incoherent ICS and the coherent high-gain ICS schemes gives the following ratio:

$$\frac{N_{\mathrm{ph,coherent}}^{\mathrm{single-electron}}}{N_{\mathrm{ph,\ incoherent}}^{\mathrm{single-electron}}} = \frac{\rho_{\mathrm{FEL}} E_{\mathrm{e}}/E_{\mathrm{ph}}}{\frac{2}{3\sqrt{3}}\frac{r_{\mathrm{e}}}{\lambda_c}} = \frac{\rho_{\mathrm{FEL}}}{\frac{2}{3\sqrt{3}}\frac{r_{\mathrm{e}}}{\lambda_c}}\frac{\gamma_{\mathrm{e}} m_{\mathrm{e}} c^2}{\frac{2\pi\hbar c}{\lambda_x}} = \frac{\rho_{\mathrm{FEL}}}{\frac{2}{3\sqrt{3}}\frac{r_{\mathrm{e}}}{\lambda_c}}\frac{\gamma_{\mathrm{e}} m_{\mathrm{e}} c^2}{2\pi\hbar c}\frac{\lambda_L}{4\gamma_{\mathrm{e}}^2} = \frac{1}{\left(\frac{2\pi\hbar}{m_{\mathrm{e}} c}\right)}\frac{\rho_{\mathrm{FEL}}}{\frac{2}{3\sqrt{3}}\frac{r_{\mathrm{e}}}{\lambda_c}}\frac{\lambda_L}{4\gamma_{\mathrm{e}}}$$

$$= \frac{3\sqrt{3}}{8}\frac{\lambda_L}{r_{\mathrm{e}}}\frac{\rho_{\mathrm{FEL}}}{\gamma_{\mathrm{e}}}$$

$$\frac{N_{\mathrm{ph,coherent}}^{\mathrm{single-electron}}}{N_{\mathrm{ph,\ incoherent}}^{\mathrm{single-electron}}} = \frac{3\sqrt{3}}{8}\frac{\lambda_L}{r_{\mathrm{e}}}\frac{\rho_{\mathrm{FEL}}}{\gamma_{\mathrm{e}}}, \tag{S79}$$

Therefore, the number of photons produced per electron in the incoherent scheme is 3-5 orders of magnitude lower than the coherent high-gain ICS scheme. The saturation power of the incoherent scheme:

$$P_{\mathrm{incoherent\ ICS}}^{(\mathrm{peak})} = P_{\mathrm{coherent\ ICS}}^{(\mathrm{peak})}\left(\frac{N_{\mathrm{ph,coherent}}^{\mathrm{single-electron}}}{N_{\mathrm{ph,\ incoherent}}^{\mathrm{single-electron}}}\right)^{-1} = P_{\mathrm{coherent\ ICS}}^{(\mathrm{peak})}\frac{8}{3\sqrt{3}}\frac{r_{\mathrm{e}}}{\lambda_L}\frac{\gamma_{\mathrm{e}}}{\rho_{\mathrm{FEL}}}$$

One should note that the total number of photons emitted in the incoherent ICS scheme (as found in Eq. (S78)) has an emission cone of $0.1\gamma_{\mathrm{e}}^{-1}$, and emission energy of ~1%, which is much broader than the coherent ICS scheme. In particular, the incoherent ICS brightness is given by [3]:

$$B_{\mathrm{incoherent\ ICS}}^{(\mathrm{peak})} \approx 1.5\times 10^{-3}\frac{1}{8\pi^3}\frac{N_{\mathrm{e}}}{\tau_p \epsilon_x \epsilon_y}\frac{N_L}{\sigma_L^2}\sigma_T$$

$$B_{\mathrm{incoherent\ ICS}}^{(\mathrm{peak})} \approx B_{\mathrm{coherent\ ICS}}^{(\mathrm{peak})}\left(\frac{N_{\mathrm{ph,coherent}}^{\mathrm{single-electron}}}{N_{\mathrm{ph,\ incoherent}}^{\mathrm{single-electron}}}\right)^{-1} \times (1.5\times 10^{-3}),$$

where the second term comes from the number of photons produced per single electron and the third term comes from the lower linewidth and spatial dispersion. Figure 4 in the main text shows the peak brightness and saturation power for the two schemes as a function of the emission energy. The high-gain ICS peak brightness is up to 6-8 orders of magnitude higher than the incoherent scheme: ~3-5 orders of magnitude arise from the higher number of photons emitted per a single electron, and additional 3 orders of magnitude are due to the lower linewidth and spatial dispersion.

5.6 The laser beam requirements for an electron source fulfilling the upper bound

Assuming an electron source achieving the upper bounds, the requirement on the laser beam can be significantly relaxed. For example, the laser pulse energy becomes (Eq. (S55)):

$$E_p^{(\text{laser})} \geq \frac{c\epsilon_0|E_0|^2}{2}\frac{K\lambda_L^3}{8c\rho_{\text{FEL}}^{5/2}} \geq \frac{\epsilon_0|E_0|^2}{2}\frac{16\sqrt{2}K\lambda_L^3}{K^5} = \frac{8\sqrt{2}\epsilon_0|E_0|^2\lambda_L^3}{K^4} = \frac{8\sqrt{2}\epsilon_0|E_0|^2\lambda_L^3}{\left(\frac{eE_0\lambda_L}{2\pi m_e c^2}\right)^4}$$

$$= \frac{8\sqrt{2}\epsilon_0}{\left(\frac{e}{2\pi m_e c^2}\right)^4}\frac{1}{\lambda_L E_0^2} = 128\pi^4\sqrt{2}\left(\frac{m_e c^2}{e}\right)^4\epsilon_0\frac{1}{\lambda_L E_0^2}$$

Specifically, if we choose $\rho_{\text{FEL}} = 10^{-3}$, a LWIR laser with a $\lambda_L = 10\mu\text{m}$ wavelength and $K = 0.09$, we get a required laser pulse energy of ~1J, a few orders of magnitude lower requirement on the laser pulse energy relative to state-of-the-art electron sources (section 6). In addition, the laser pulse parameters (energy, power, and duration) are independent of the electron source parameters and the emitted X-ray energy, in contrast to the non-ideal electron source.

6. State-of-the-art sources

6.1 EUV and water-window sources

In this section, we discuss the experimental implementation feasibility of a high-gain ICS scheme with either state-of-the-art or near-future electron and laser beam sources. We will examine two high-gain ICS schemes. The first is for producing an EUV beam with a lasing wavelength of 13.5nm, which is required for applications such as lithography and wafer inspection [11][12]. This scheme uses a CO_2 laser in the LWIR spectrum ($\lambda_L = 10\mu m$). The second scheme is for producing a soft X-ray beam in the water-window spectrum, which has applications in biological sample imaging [13]. This scheme uses a NIR laser ($\lambda_L = 1\mu m$).

The electron source parameters used for the analysis are based on a recent report of the parameters required for future electron sources [14]. The target parameters are shown in Table S4. Due to the strict requirements on the electron beam emittance and the energy spread, we will focus on the UEM and the XFEL sources. The UEM source has low normalized emittance and energy spread, which makes it suitable for soft X-ray applications, yet its relatively low peak current limits the emitted beam power. The XFEL source has a much larger electron charge and peak current, yet with higher emittance, which limits the maximal emission energy of the high-gain ICS scheme.

The normalized brightness of the sources is defined by [10]:

$$B_n = \frac{I_e}{\pi^2 \epsilon_n^2} \tag{S80}$$

The normalized brightness values are shown in Table S4. Comparing these values to the quantum-mechanical limit gives at least five orders below the quantum-mechanical theoretical limit (Eq. (S57)).

	UED	UEM	XFEL (cold)	XFEL (warm)
Charge	20 fC – 0.5 pC	0.5-1 pC	200 pC	200 pC
Bunch length	10 fs	10 ps	1 ps	<1 ps
Energy spread	10^{-2}	10^{-5}	10^{-4}	10^{-4}
Normalized Emittance	<5 nm	<2 nm	100 nm	50 nm
Repetition Rate	Process dependent	100 Hz	1 MHz	120 Hz
Peak current [A]	50	0.1	200	200
Normalized Brightness $\left[\frac{C}{s\ m^2\ rad^2}\right]$	2×10^{17}	2.5×10^{15}	2×10^{15}	8×10^{15}

Table S4: Target parameters for future electron sources. Taken from [5]

The electron beam emittance sets an upper limit on the X-ray wavelength due to the condition for transverse coherence (Eq. (S16)). On the one hand, the normalized beam emittance scales as γ_e^{-1}, while on the other hand, the X-ray wavelength scales as γ_e^{-2}. In other words, the following holds:

$$\frac{\epsilon_n}{\beta\gamma_e} < \frac{\lambda_x}{4\pi} = \frac{\lambda_L}{16\pi\gamma_e^2}, \tag{S81}$$

Rearranging the terms, we derive the upper limit for the electron energy:

$$\gamma_e < \frac{\lambda_L}{16\pi\epsilon_n}, \tag{S82}$$

Let us consider as an example the UEM and XFEL electron sources, as specified by Table S4. The UEM-based electron source has a beam emittance of ϵ_n =2 nm-rad and energy spread of 10^{-5}. For the laser source, we will use a laser wavelength of $\lambda_L = 1\mu m$. The maximal electron energy that will satisfy the condition specified in Eq. (S82) is ~5.5MeV, i.e., the lowest X-ray emission wavelength would be ~2.5nm and X-ray energy of ~500eV. Therefore, a state-of-the-art UEM electron source can be appropriate for generating coherent ICS X-ray beam in the water-window spectrum. The XFEL electron source does not meet the requirement for a transverse coherent emission for an emission energy of 13.5nm. However, the electron micro-bunching requirements hold, and the high charge density results in high beam power.

Table S5 shows the typical requirements of the laser beam for EUV source. It assumes the parameters of the XFEL electron source with an electron energy beam of 6.96 MeV, as specified in Table 3. The laser system is LWIR ($\lambda_L = 10\mu m$), based on a CO_2 laser. The X-ray beam parameters (the Pierce parameter, the FEL gain length, the interaction length, saturation power, and peak brightness) are compared as a function of the undulator parameter strength. For higher undulator parameter values, the Pierce parameter, the peak power, and the peak brightness increase. Therefore, larger laser intensities are preferable to achieve higher emission saturation power as far as $K \ll 1$ (the linear ICS regime). However, for higher undulator parameters, the intensity fluctuations during the pulses become a limiting factor on the X-ray emission linewidth (Eq. (S43)). If the intensity fluctuation can't be met, lower laser intensities should be used. The CO_2 laser requirements are a ~TW pulse power, with tens to a few hundredths' picosecond pulse duration, a beam waist of hundredths micrometer, and pulse energy of tens to 100 Joule. These parameters can be met with existing CO_2 laser technology [15][16]. This scheme can produce an EUV beam with a peak power of hundredths of kW up to 1MW, comparable to plasma-based sources. Its peak brightness is ~10^{27} $\left[\frac{\text{photons}}{\text{s mm}^2\ \text{mrad}^2\ 0.1\%BW}\right]$, up to 8 orders of magnitude higher than state-of-the-art incoherent ICS schemes [3]. However, this value is 6 orders of magnitude below the undulator-based FEL. The difference arises from the lower electron energy beam (E_{beam}) of ~3 orders of magnitude, a lower electron source current (2 orders of magnitude), and an order lower in the Pierce parameter ρ_{FEL}.

	Parameter	EUV-1	EUV-2	EUV-3	EUV-4
Electron source	β_{av}	1 cm	1 cm	1 cm	3 cm
	Spot size at IP	6 μm	6 μm	6 μm	10 μm
	Beam divergence	0.6 mrad	0.6 mrad	0.6 mrad	0.35 mrad
Laser beam	Laser wavelength	10 μm (LWIR)	10 μm (LWIR)	10 μm (LWIR)	10 μm (LWIR)
	Undulator parameter	**0.2**	**0.1**	**0.07**	**0.04**
	Electric field	65 GV/m	32 GV/m	22 GV/m	13 GV/m
	Maximal allowed intensity noise $\left(\frac{\Delta I_0}{I_0}\right)$	1.5%	4%	6%	4%
	Pulse power	2.5 TW	650 GW	200 GW	120 GW
	Pulse duration	30 ps	50 ps	60 ps	180 ps
	Pulse energy	80 J	30 J	12 J	20 J
X-ray beam	Wavelength	**13.5 nm**	**13.5 nm**	**13.5 nm**	**13.5 nm**
	Energy	92 eV	92 eV	92 eV	92 eV
	Pierce parameter ρ_{FEL}	6×10^{-4}	$\sim4\times10^{-4}$	$\sim3\times10^{-4}$	$\sim10^{-4}$
	FEL gain length L_{g0}	0.5 mm	0.7 mm	0.8 mm	2 mm
	Interaction length L_{sat}	1 cm	1.5 cm	2 cm	6 cm
	Saturation power	**~ 1 MW**	**~ 500 kW**	**~ 400 kW**	**~ 100 kW**
	Peak brightness	$\sim2\times10^{27}$	$\sim10^{27}$	$\sim9\times10^{26}$	$\sim5\times10^{26}$

Table S5: Different setups for an EUV source based on a high-gain ICS scheme. When using lower laser pulse power, the Pierce parameter drops, and the electron energy spread requirement becomes stricter.

Table S6 shows the typical requirements for a soft X-ray source in the water-window spectrum ($\lambda_x = 2.6$ nm, $\hbar\omega_x \approx$ 470eV) based on a UEM electron source. The proposed source uses an NIR laser with a $\lambda_L = 1\mu$m wavelength and an electron beam energy of 5MeV. Different configurations are compared as a function of the undulator parameter. Like the previous source, using higher values of the undulator parameter increases the Pierce parameter and the saturation power and peak brightness at the expense of stricter requirements on the allowed laser beam fluctuations. However, in this scheme, the maximal allowed intensity noise is an order of magnitude lower than the EUV source due to the lower Pierce parameter. In addition, the required pulse power and pulse energy are two orders of magnitude higher than the previous scheme due to the shorter emission wavelength and the lower electron charge density of the electron source. The source saturation power and peak brightness are significantly lower than the EUV source proposed

previously (~5 orders of magnitude lower saturation power and ~3 orders of magnitude lower peak brightness), mainly due to the much lower electron beam peak current (~3 orders of magnitude). However, relative to state-of-the-art incoherent ICS schemes, the peak brightness of this source is ~5 orders of magnitude higher, even when using the relatively low electron pulse charge of the UEM source. In this scheme, quantum-recoil effects become prominent since the quantum recoil parameter (Eq. (S33)) is $q \approx 2-5$. This scheme can be an interesting experimental realization for quantum effects in a high-gain regime.

	Parameter	**Soft X-ray - 1**	**Soft X-ray - 2**	**Soft X-ray - 3**
Electron source	β_{av}	1 cm	1 cm	1 cm
	Spot size at IP	1.5 μm	1.5 μm	1.5 μm
	Beam divergence	0.14 mrad	0.14 mrad	0.14 mrad
Laser beam	Laser wavelength	1 μm (NIR)	1 μm (NIR)	1 μm (NIR)
	Undulator parameter	**0.2**	**0.1**	**0.07**
	Electric field	650 GV/m	320 GV/m	220 GV/m
	Maximal allowed intensity noise $\left(\frac{\Delta I_0}{I_0}\right)$	0.1%	0.23%	0.4%
	Pulse power	110TW	25TW	16TW
	Pulse duration	40ps	70ps	85ps
	Pulse energy	4.5kJ	1.8kJ	1.3kJ
X-ray beam	Wavelength	**2.6 nm**	**2.6 nm**	**2.6 nm**
	Energy	465 eV	472 eV	473 eV
	Pierce parameter ρ_{FEL}	4×10^{-5}	2.5×10^{-5}	1.8×10^{-5}
	FEL gain length L_{g0}	0.6 mm	1mm	1.25mm
	Interaction length L_{sat}	1.2 cm	2cm	2.5cm
	Saturation power	**~ 20 W**	**~~ 10 W**	**~~ 5 W**
	Peak brightness	$\sim 1.6 \times 10^{24}$	$\sim 1.1 \times 10^{24}$	$\sim 8 \times 10^{23}$

Table S6: Different setups for a water-window soft X-ray source based on a high-gain ICS scheme. When using lower laser pulse power, the Pierce parameter drops, and the electron energy spread requirement becomes stricter.

6.2 Maximal high-gain ICS emission energy

Here we find the connection between the maximal allowed emission energy as a function of the electron source brightness and the laser beam energy (Figure 4(a) in the main paper). First, we start with the connection between the electron charge density and the electron normalized brightness:

$$n_{\mathrm{e}} = \frac{1}{ec}\frac{I_{\mathrm{e}}}{2\pi\sigma_x\sigma_y} = \frac{1}{ec}\frac{I_{\mathrm{e}}}{\frac{2\pi\epsilon_n^2}{\gamma_{\mathrm{e}}^2\sigma_{x'}^2}} = \frac{1}{ec}\frac{\pi}{2}B_n\gamma_{\mathrm{e}}^2\sigma_{x'}^2$$

We use the relation between the electron beam divergence and the beam emittance and beta function $\sigma_{x'}^2 = \frac{\epsilon}{\beta_{\mathrm{av}}} = \frac{\epsilon_n}{\gamma_{\mathrm{e}}\beta_{\mathrm{av}}}$:

$$n_{\mathrm{e}} = \frac{1}{ec}\frac{\pi}{2}B_n\gamma_{\mathrm{e}}^2\sigma_{x'}^2 = \frac{1}{ec}\frac{\pi}{2}B_n\frac{\gamma_{\mathrm{e}}\epsilon_n}{\beta_{\mathrm{av}}}$$

We assume the electron source emittance is set to fulfill the condition of spatially coherent emission, i.e., $\epsilon_n = \epsilon\gamma_{\mathrm{e}} = \frac{\lambda_x}{4\pi}\gamma_{\mathrm{e}} = \frac{\lambda_L}{16\pi\gamma_{\mathrm{e}}}$:

$$n_{\mathrm{e}} = \frac{1}{ec}\frac{\pi}{2}B_n\frac{\gamma_{\mathrm{e}}\epsilon_n}{\beta_{\mathrm{av}}} = \frac{1}{32}\frac{1}{ec}B_n\frac{\lambda_L}{\beta_{\mathrm{av}}}$$

Since the beta function should satisfy $\beta_{\mathrm{av}} \approx \frac{1}{2}L_{\mathrm{sat}} \approx \frac{\lambda_u}{2\rho_{\mathrm{FEL}}} = \frac{\lambda_L}{4\rho_{\mathrm{FEL}}}$, we get:

$$n_{\mathrm{e}} = \frac{1}{32}\frac{1}{ec}B_n\frac{\lambda_L}{\beta_{\mathrm{av}}} = \frac{1}{8}\frac{1}{ec}B_n\rho_{\mathrm{FEL}}$$

Therefore, we get the following relation between the electron normalized emittance to the electron charge density:

$$B_n = \frac{8ec}{\rho_{\mathrm{FEL}}}n_{\mathrm{e}}, \tag{S83}$$

If we compare the result to the quantum-mechanical bound of the electron-normalized beam emittance (Eq. (S57)), we get that the bound is fulfilled for $n_{\mathrm{e}} = \frac{1}{4}\frac{1}{\lambda_c^3}\rho_{\mathrm{FEL}}\Delta\gamma_{\mathrm{e}}$. Therefore, figure 4(a) in the main text was produced by setting the variables n_{e} and γ_{e} and deriving $\rho_{\mathrm{FEL}}$and B_n by Eq. (S83). One should note that Eq. (S83) derivation is under the assumption of transverse coherence emission.

7. Low-gain inverse Compton scattering

7.1 The inverse Compton scattering oscillator scheme

In this section, we analyze the performance of the low-gain ICS (ICS oscillator) scheme. We analyze the following: 1) the energy spread impact on the gain in each pass (section 7.2). 2) the quantum-recoil effect (section 7.3). 3) the requirements on the laser beam pulse (section 7.4). 4) 5) the emission energy upper bound supported by the scheme (section 7.5).

In the ICS oscillator scheme, the X-ray wave gains a small amount of power in each pass. After many passes, the X-ray wave intensity increases exponentially and saturates. The power increase can be described by:

$$\begin{aligned} P_1 &= P_s \\ P_n &= R(1+G)P_{n-1} + P_s, \qquad n > 1, \end{aligned} \tag{S84}$$

where P_s is the spontaneous emission, R represent the total loss due to mirrors and focusing devices, and G is the FEL gain. By Madey theory, the gain in each pass is given by [17][6]:

$$G(\xi) = -\frac{\pi e^2 K^2 N_u^3 \lambda_u^2 n_\mathrm{e}}{4\epsilon_0 m_\mathrm{e} c^2 \gamma_\mathrm{e}^3} \frac{d}{d\xi}\left(\frac{\sin^2\xi}{\xi^2}\right) = -\pi^2 r_\mathrm{e} \frac{K^2 N_u^3 \lambda_u^2 n_\mathrm{e}}{\gamma_\mathrm{e}^3} \frac{d}{d\xi}\left(\frac{\sin^2\xi}{\xi^2}\right), \tag{S85}$$

where K is the undulator parameter, λ_u is the undulator period, n_e is the electron density, η is the relative energy deviation between the electron beam and the resonance energy of the cavity and $\xi = 2\pi N_u \eta$ is the detuning parameter:

$$\xi = 2\pi N_u \frac{(\gamma_\mathrm{e} - \gamma_r)}{\gamma_r} = 2\pi N_u \eta, \tag{S86}$$

where $E_\mathrm{e} = \gamma_\mathrm{e} mc^2$ is the electron energy, and γ_r represents the resonator wavelength as specified by Eq. (S3). Electrons with positive η (i.e., higher energy than the resonator energy) enhance the intensity of the light wave, while those with negative η reduce it.

Figure S9 shows the typical energy transfer as a function of the detuning parameter for the following parameters: electron beam density of $n_\mathrm{e} = 10^{21}\ \left[\frac{1}{\mathrm{m}^3}\right]$, number of undulation periods of $N_u = 3000$, undulation parameter of $K = 0.1$, Lorentz factor of $\gamma_\mathrm{e} = 19.56$, and NIR laser wavelength of $\lambda_L = 1\mu\mathrm{m}$. In this configuration, the emitted X-ray wavelength is $\lambda_\mathrm{x} \approx 6.5\text{Å}$ (~1900eV), and the interaction length is $N_u\lambda_u$~1.5mm. For this configuration, the maximal energy transfer in a single pass is ~13%. The peak gain is achieved for a relative energy spread of $\eta \approx \frac{1.3}{2\pi N_\mathrm{u}}$, defining the allowed energy spread of the electron beam to be below this value (RMS). The relative energy deviation specifies the allowed X-ray wave linewidth and is analogous to the Pierce parameter in the high-gain regime, i.e., the requirements that depend on the Pierce parameter can be replaced by $\eta \approx \frac{1.3}{2\pi N_\mathrm{u}}$. Therefore, longer interaction length will increase the gain in each pass at the expense of stricter requirements of the electron beam energy spread.

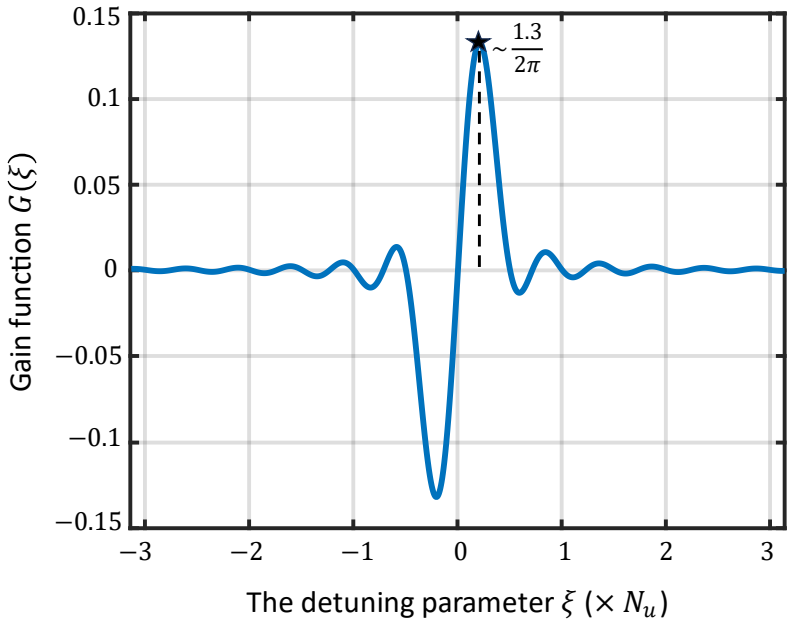

Figure S9: The coherent ICS low gain function as a function of the detuning parameter. This graph was produced with the following parameters: $\gamma_e = 19.56, \lambda_L = 1\ \mu m, N_u = 3000, n_e = 10^{21}\ \left[\frac{1}{m^3}\right], K = 0.1$. The interaction length is ~1.5 mm for this configuration.

The exponential growth of the intracavity radiation power does not continue indefinitely. Rather, the power of the X-ray beam eventually becomes large enough to trap electrons in the ponderomotive potential and then rotate them to an absorptive phase where they extract energy from the field. The saturation power is given by:

$$P_{\mathrm{sat}} = \frac{P_{\mathrm{e}}}{2N_{\mathrm{u}}(1-R)} \tag{S87}$$

where P_{e} is the electron beam power. Eq. (S87) is analogous to Eq. (S74), where the Pierce parameter ρ_{FEL} is replace by N_{u}^{-1}. Compared to SASE from a high-gain FEL, the pulse intensity of an X-FELO is lower due to the lower electron power in each pulse, but its spectrum is narrower by more than three orders of magnitude due to the narrow energy bandwidth transfer of the crystals and can be low as a few meV [44]. Therefore, the peak brightness is rather similar between the ICS oscillator and the coherent ICS in the high-gain regime.

7.2 Electron energy spread

The gain function (as described by Eq. (S85)) depends on the detuning parameter ξ and achieves its maximal value for $\xi \sim \frac{1.3}{2\pi N_u}$. Due to the electron energy spread, the effective gain will be smaller. This value can be seen as analogous to the Pierce parameter in the high-gain regime, yet with a different physical meaning. In the high-gain ICS regime, the energy spread ruins the micro-bunching process, preventing the exponential growth in the emitted intensity. On the other hand, in the low-gain scheme, the greater energy spread decreases the effective gain per pass, resulting in a lower saturation power of the X-ray beam (or more strict requirements on the reflectivity of the oscillator cavity).

To consider the electron energy spread, we perform averaging of the gain as a function of the electron energy spread random variable. Let us denote the term in the gain function that depends on the detuning parameter:

$$h(\xi) = \frac{d}{d\xi}\left(\frac{\sin^2\xi}{\xi^2}\right) = \frac{2\xi\cos\xi\sin\xi - 2\sin^2\xi}{\xi^3}, \tag{S88}$$

We write the electron energy spread probability function as a Gaussian random variable with a standard deviation of $\sigma_\xi = 2\pi N_u(\sigma_E/E_r)$, where σ_E/E_r is the effective electron energy spread, which considers also the electron beam divergence, as specified by Eq. (S29):

$$p_{\sigma_E}(\xi) = \frac{1}{\sqrt{2\pi(2\pi N_u)^2(\sigma_E/E_r)^2}}\exp\left(-\frac{(\xi-1)^2}{2(2\pi N_u)^2(\sigma_E/E_r)^2}\right), \tag{S89}$$

Therefore, the gain function as a function of the electron energy spread is given by:

$$G_0 = E[G(\xi)] = -\pi^2 r_e \frac{K^2 N_u^3 \lambda_u^2 n_e}{\gamma_e^3} E[h(\xi)], \tag{S90}$$

where:

$$E[h(\xi)] = \int d\xi\, h(\xi)\, p_{\sigma_E}(\xi)$$

Figure S10(a) shows the function $h(\xi)$ and $p_{\sigma_E}(\xi)$ for different energy spread values as a function of the detuning parameter ξ. Figure S10(b) shows the mean value of the gain $E[h(\xi)]$ for various electron energy spreads. The number of undulation periods used to produce the graph is $N_u = 1000$. As can be seen, the effective electron energy spread limits the number of undulation periods. In X-ray FEL oscillator designs, the number of undulation periods used is such that the effective electron energy spread is larger than the allowed linewidth, i.e., $\frac{\sigma_E}{E_r} > \frac{1}{2\pi N_u}$ [18][19]. However, in the low-gain ICS oscillator scheme, we choose the design parameters such that $\frac{\sigma_E}{E_r} < \frac{1}{2\pi N_u}$. In this case, the gain function can be approximated by:

$$G_0 \approx \frac{\pi^2}{2} r_e \frac{K^2 N_u^3 \lambda_u^2 n_e}{\gamma_e^3}, \tag{S91}$$

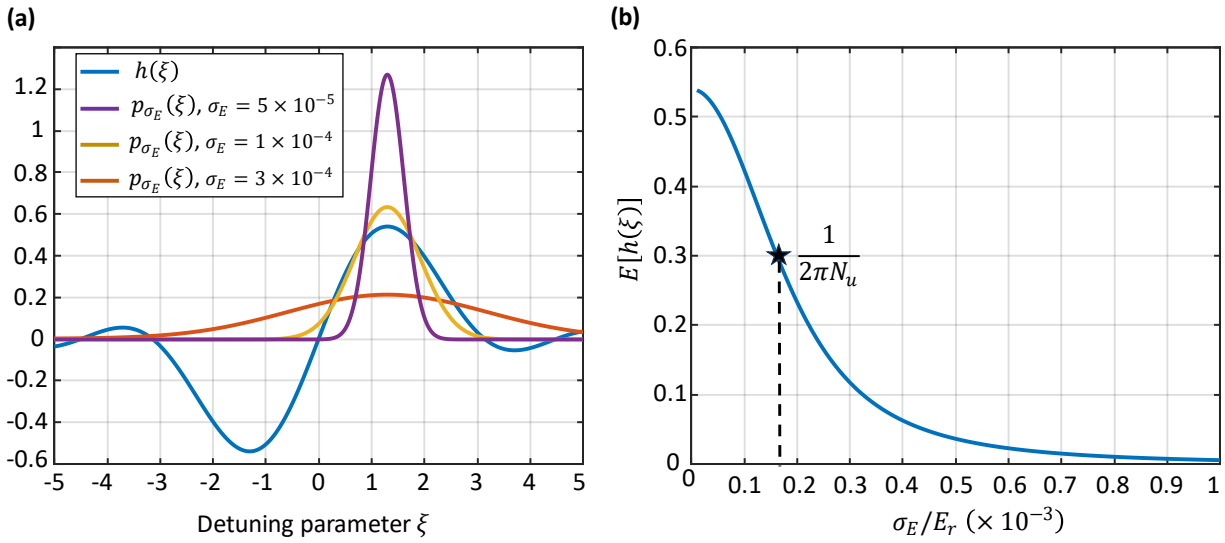

Figure S10: The electron energy spread impact on a low-gain ICS scheme. The graphs were produced for $N_u = 1000$, $\lambda_L = 10\ \mu m$, $n_e = 2 \times 10^{21}[1/m^3]$, and $K = 1$. **(a)** $h(\xi)$ (Eq. (S88)) and $p_{\sigma_E}(\xi)$ (Eq. (S89)) as a function of the detuning parameter ξ. **(b)** The normalized gain in a single pass as a function of the electron energy spread.

7.3 Quantum recoil

As discussed in section 3.50, quantum recoil becomes considerable when the mean energy loss of an electron is higher than the allowed emission linewidth. This phenomenon is significant in the coherent high-gain regime since a single electron can lose energy that is larger than $\rho_{\mathrm{FEL}}\gamma_{\mathrm{e}}m_{\mathrm{e}}c^2$ (Eq. (S33)). Similar phenomenon would occur in the low-gain ICS regime when the incoming X-ray beam power is large enough to trap the electron in the pondermotive potential.

At the start of the ICS oscillator process, the X-ray emission is mostly spontaneous and is similar to the regular incoherent ICS scheme. In this case, the number of electrons that emit photons is much smaller than unity (section 5.5); thus, quantum recoil effects are negligible. However, as the X-ray wave gains power, its interaction with the fresh electron beam pulses is stronger, resulting in higher photon production per single electron. We consider the number of additional X-ray photons produced in the last rounds. We assume a moderate increase in each pass, i.e., $G_0 \ll 1$. Following Eq. (S87):

$$P_{\mathrm{sat}} = \frac{P_{\mathrm{e}}}{2N_{\mathrm{u}}(1-R)} \rightarrow N_{\mathrm{sat}}\hbar\omega_x = \frac{N_{\mathrm{e}}\gamma_{\mathrm{e}}m_{\mathrm{e}}c^2}{2N_u(1-R)}$$

Therefore, in the last rounds, assuming a gain of G_0, the number of photons produced per single electron (for a fresh electron beam) are:

$$N_{\mathrm{ph}}^{\text{single electron}} \approx G_0 \frac{1}{2N_u(1-R)}\frac{E_{\mathrm{e}}}{E_{\mathrm{ph}}}, \tag{S92}$$

We define the quantum recoil parameter in the low-gain regime analogously to the high-gain regime, to be:

$$q_{\mathrm{recoil}}^{(\mathrm{low-gain})} = 2\pi N_u \frac{\hbar\omega_x}{\gamma_{\mathrm{e}}m_{\mathrm{e}}c^2}, \tag{S93}$$

where ρ_{FEL} was replaced by $(2\pi N_u)^{-1}$ due to the accepted linewidth broadening. Combining Eq. (S92) and Eq. (S93):

$$N_{\mathrm{ph}}^{\text{single electron}} = \frac{G_0}{1-R}\frac{\pi}{q_{\mathrm{recoil}}}$$

The quantum recoil effect becomes dominant in the last rounds of the ICS oscillator scheme for $q_{\mathrm{recoil}} \approx 1$. Therefore, with a similar argument as in the high-gain ICS, the Pierce parameter (the allowed linewidth in the high-gain ICS scheme) is replaced by $(2\pi N_u)^{-1}$ (the allowed linewidth in the low-gain ICS scheme). When comparing the allowed energy broadening of the low-gain and the high-gain schemes, the low-gain ICS scheme has a relative advantage over the high-gain ICS scheme due to the shorter interaction length. Figure S11(a) shows the Pierce parameter and the energy linewidth of the low-gain ICS regime as a function of the emitted X-ray energy. While in the high-gain scheme, the linewidth decreases for higher X-ray energies (Eq. (S20)), the linewidth in the low-gain regime remains constant and depends only on the number of undulation periods.

Figure S11(b) compares the quantum recoil of the high-gain and the low-gain schemes for a LWIR laser. While in the high-gain ICS regime, the quantum recoil becomes dominant at ~2keV, in the low-gain ICS regime it affects only at 12keV.

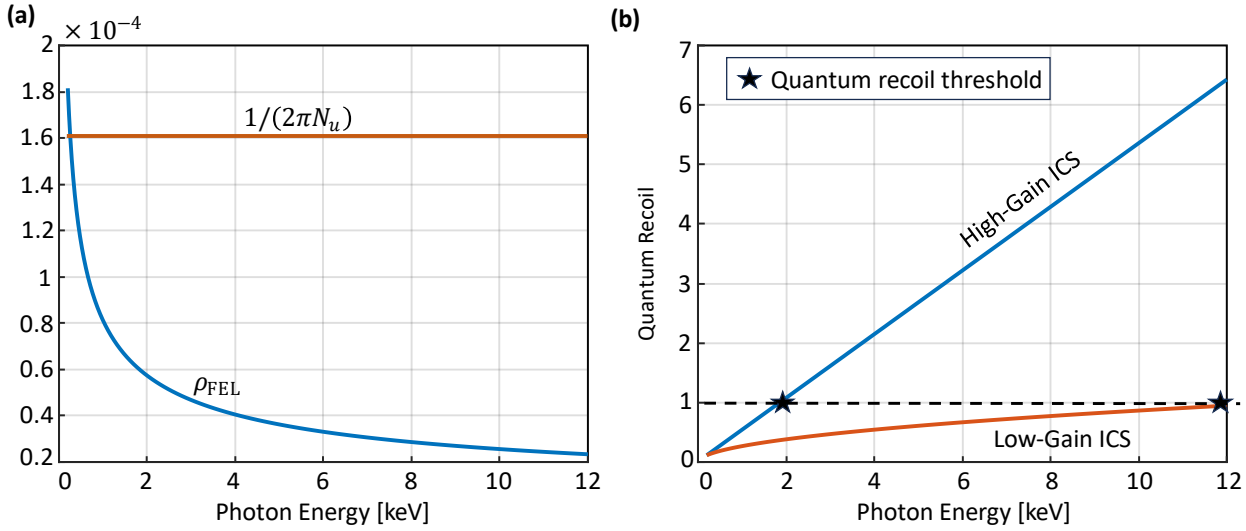

Figure S11: Quantum recoil effects comparison between high-gain ICS and low-gain ICS. **(a)** The Pierce parameter of the high-gain ICS and the analogous $(2\pi N_u)^{-1}$ parameter for the low-gain oscillator scheme as a function of the X-ray energy. **(b)** The quantum recoil-value for the high-gain and low-gain ICS as a function of the X-ray energy.

7.4 Laser pulse requirements

The laser pulse requirements are different between the high-gain and the low-gain schemes. In the high-gain ICS scheme, the requirements are necessary for fulfilling the conditions for electron micro-bunching, whereas, in the low-gain ICS scheme, the laser pulse is necessary to increase the effective gain in each pass. Since the interaction length is much shorter in the low-gain scheme, the pulse duration requirement is lower by an order of magnitude. Moreover, the laser beam waist and the pulse power can be lower due to more relaxed conditions on the beam divergence. Following the discussion of section 7.2, the allowed linewidth broadening of the beam, due to the electron spread and the laser fluctuations, should be restricted by $\sim\frac{1.3}{2\pi N_u}$. The derivation for the laser parameters bounds is similar in the low-gain ICS regime compared with section 4, where the Pierce parameter is replaced by $\rho_{\mathrm{FEL}}\sim\frac{1.3}{2\pi N_u}$ and the interaction length is replaced by $L_{\mathrm{sat}} = N_u\lambda_u$. Thus, the laser fluctuations should satisfy:

$$K^2\frac{\Delta K}{K} \leq \frac{1.3}{4\pi N_u}$$

Since $\frac{\Delta K}{K} = \frac{\Delta E_0}{E_0}$, we obtain the following requirement (similarly to the derivation of Eq. (S45)):

$$\frac{K^2}{8}\left(\frac{N_u\lambda_u}{z_R}\right)^2 \leq \frac{1.3}{4\pi N_u}$$

Therefore, we get the following bound on the laser Rayleigh length:

$$z_R \geq \frac{KN_u\lambda_u}{\sqrt{1.3}}\sqrt{\frac{\pi N_u}{2}} \approx \frac{K\lambda_L}{2}N_u^{3/2}, \tag{S94}$$

And the beam waist size is:

$$w_0 = \sqrt{\frac{z_R\lambda_L}{\pi}} \geq \sqrt{\frac{\left(\frac{K\lambda_L}{2}N_u^{3/2}\right)\lambda_L}{\pi}} = \lambda_L\sqrt{\frac{KN_u^{3/2}}{2\pi}}, \tag{S95}$$

The beam power bound is:

$$P_0 = \frac{c\epsilon_0 E_0^2}{2}\pi w_0^2 = \frac{c\epsilon_0 E_0^2}{2}z_R\lambda_L \geq \frac{c\epsilon_0 E_0^2}{2}\frac{K\lambda_L^2}{2}N_u^{3/2}, \tag{S96}$$

As in the high-gain derivation, we assume the laser beam system is optimized to the transform-limited bound; thus, the pulse duration requirement comes from the linewidth requirement, i.e., for $\frac{\Delta\omega_L}{\omega_L} \leq \frac{1}{4\pi N_u}$, we get:

$$\tau_p\Delta\omega = 1/2 \rightarrow \tau_p \geq \frac{1}{\frac{2\omega_L}{(4\pi N_u)}} = \frac{2\pi N_u}{\frac{2\pi}{\lambda_L}c} = \frac{N_u\lambda_L}{c}$$

$$\tau_p \geq \frac{N_u\lambda_L}{c}, \tag{S97}$$

Finally, the laser beam energy bound is given by:

$$E_p^{(\text{laser})} = P_0\tau_p \geq \frac{c\epsilon_0 E_0^2}{2}\frac{K\lambda_L^2}{2}N_u^{3/2}\frac{N_u\lambda_L}{c} = \frac{\epsilon_0 E_0^2}{4}K\lambda_L^3 N_u^{5/2}, \tag{S98}$$

One should note that in contrast to the high-gain regime, the laser requirements are independent of the electron source energy nor the emission wavelength but only on the number of undulation periods N_u. For a scheme of an LWIR laser source with a wavelength of $\lambda_L = 10\mu\text{m}$, number of undulation periods of $N_u = 1000$ and undulator parameter of $K = 0.1$, the requirements are laser pulse power of $P_0 = 200\text{GW}$, laser pulse duration of $\tau_p = 35\text{ps}$ and total laser pulse energy of $E_p^{(\text{laser})} = 7\text{J}$. These requirements are much less strict than the high-gain scheme requirements and are not scaling up with higher X-ray energies.

7.5 Maximal low-gain ICS emission energy

Here, we show the derivation and assumptions used to produce Figure 4(b) in the main text. We assume the following: 1) the electron beam emittance achieves the condition for a transverse coherent emission, i.e., $\epsilon_n = \frac{\lambda_x}{4\pi}\gamma_\mathrm{e}$. 2) the average beta function equals half the interaction length, i.e., $2\beta_\mathrm{av} \approx \frac{N_u\lambda_L}{2}$. 3) the low-gain approximation is valid (Eq. (S85)), i.e., $G < 2$. 4) the electron source energy spread is lower than $\frac{\sigma_E}{E_r} < \frac{1}{2\pi N_u}$. For these assumptions, the approximation of Eq. (S91) is valid since:

$$\sigma_{x'}^2 = \frac{\epsilon_x}{\beta_\mathrm{av}} = \frac{2\epsilon_x}{N_u\lambda_u} = \frac{2\frac{\lambda_x}{4\pi}}{N_u\lambda_u} \approx \frac{1}{2\pi N_u}\frac{1}{2\gamma_\mathrm{e}^2} \rightarrow (\gamma_\mathrm{e}\sigma_{x'})^2 \approx \frac{1}{4\pi N_u}$$

Thus, the energy spread due to the beam divergence is negligible. For the assumptions above, we represent the electron-normalized brightness in the same manner as we have derived in Eq. (S83):

$$B_n = 8ecN_u n_\mathrm{e}, \tag{S99}$$

The electron source normalized brightness representation is analogous to the representation in the high-gain ICS case, where $\rho_\mathrm{FEL} = \frac{1}{N_u}$.

To achieve a net gain in each pass of the ICS oscillator, we require $R(1+G_0) > 1$. Therefore substituting Eq. (S91) for this requirement:

$$R(1+G_0) > 1 \rightarrow R\left(1 + \frac{\pi^2}{2} r_\mathrm{e}\frac{K^2 N_u^3 \lambda_u^2 n_\mathrm{e}}{\gamma_\mathrm{e}^3}\right) > 1 \rightarrow R > \frac{1}{1 + \frac{\pi^2}{2} r_\mathrm{e}\frac{K^2 N_u^3 \lambda_u^2 n_e}{\gamma_\mathrm{e}^3}}$$

$$R > \frac{1}{1 + \frac{\pi^2}{2} r_\mathrm{e}\frac{K^2 N_u^3 \lambda_u^2 n_e}{\gamma_\mathrm{e}^3}}, \tag{S100}$$

Figure 6(b) was produced for the case where the reflectivity in Eq. (S100) achieves the lower bound. The low-gain approximation is valid for $G < 2$, i.e., R>67%. One should note that if the electron source repetition rate does not match the requirements of $\frac{L_c}{c} = \frac{1}{f_R}$, and the X-ray beam will need to pass several times the cavity until the arrival of the successive fresh electron pulse, then the effective reflectivity of the scheme will be:

$$N_r = \frac{c}{L_c}\frac{1}{f_R}$$

$$R_\mathrm{eff} = R^{N_r}$$

where N_r represents the number of passes the X-ray beam makes between two adjacent electron pulses, and R is the reflectivity in a single pass.

References

[1] S. K. Ride, E. Esarey, and M. Baine, "Thomson scattering of intense lasers from electron beams at arbitrary interaction angles," *Phys. Rev. E*, vol. 52, no. 5, pp. 5425–5442, Nov. 1995, doi: 10.1103/PhysRevE.52.5425.

[2] W. J. Brown and F. V Hartemann, "Three-dimensional time and frequency-domain theory of femtosecond x-ray pulse generation through Thomson scattering," *Phys. Rev. ST Accel. Beams*, vol. 7, no. 6, p. 60703, Jun. 2004, doi: 10.1103/PhysRevSTAB.7.060703.

[3] W. S. Graves *et al.*, "Compact x-ray source based on burst-mode inverse Compton scattering at 100 kHz," *Phys. Rev. ST Accel. Beams*, vol. 17, no. 12, p. 120701, Dec. 2014, doi: 10.1103/PhysRevSTAB.17.120701.

[4] C. Pellegrini, A. Marinelli, and S. Reiche, "The physics of x-ray free-electron lasers," *Rev. Mod. Phys.*, vol. 88, no. 1, pp. 1–55, 2016, doi: 10.1103/RevModPhys.88.015006.

[5] P. Musumeci *et al.*, "Advances in bright electron sources," *Nucl. Instruments Methods Phys. Res. Sect. A Accel. Spectrometers, Detect. Assoc. Equip.*, vol. 907, pp. 209–220, 2018, doi: https://doi.org/10.1016/j.nima.2018.03.019.

[6] P. Schmüser, M. Dohlus, and J. Rossbach, *Ultraviolet and soft X-ray free-electron lasers: introduction to physical principles, experimental results, technological challenges*, vol. 229. Springer Science & Business Media, 2008.

[7] D. A. Edwards and M. J. Syphers, *An introduction to the physics of high energy accelerators*. John Wiley & Sons, 2008.

[8] C. B. Schroeder, C. Pellegrini, and P. Chen, "Quantum effects in high-gain free-electron lasers," *Phys. Rev. E*, vol. 64, no. 5, p. 56502, Oct. 2001, doi: 10.1103/PhysRevE.64.056502.

[9] A. Yariv and P. Yeh, "Optical waves in crystal propagation and control of laser radiation," 1983.

[10] M. B. Callaham, "Quantum-mechanical constraints on electron-beam brightness," *IEEE J. Quantum Electron.*, vol. 24, no. 10, pp. 1958–1962, 1988, doi: 10.1109/3.8525.

[11] C. Wagner and N. Harned, "Lithography gets extreme," *Nat. Photonics*, vol. 4, no. 1, pp. 24–26, 2010, doi: 10.1038/nphoton.2009.251.

[12] R. Bonam *et al.*, "EUV mask and wafer defectivity: strategy and evaluation for full die defect inspection," in *Extreme Ultraviolet (EUV) Lithography VII*, 2016, vol. 9776, pp. 382–389.

[13] M. Kördel *et al.*, "Laboratory water-window x-ray microscopy," *Optica*, vol. 7, no. 6, pp. 658–674, Jun. 2020, doi: 10.1364/OPTICA.393014.

[14] X. Wang, P. Musumeci, E. Lessner, and J. Goldstein, "Report of the Basic Energy Sciences Workshop on the Future of Electron Sources, September 8-9, 2016," USDOE Office of Science (SC)(United States), 2016.

[15] S. Y. Tochitsky, C. Filip, R. Narang, C. E. Clayton, K. A. Marsh, and C. Joshi, "Efficient shortening of self-chirped picosecond pulses in a high-power CO 2 amplifier," *Opt. Lett.*, vol. 26, no. 11, pp. 813–815, 2001.

[16] S. Y. Tochitsky, R. Narang, C. Filip, C. E. Clayton, K. A. Marsh, and C. Joshi, "Generation of 160-ps terawatt-power CO2 laser pulses," *Opt. Lett.*, vol. 24, no. 23, pp. 1717–1719, Dec. 1999, doi: 10.1364/OL.24.001717.

[17] J. M. J. Madey, "Relationship between mean radiated energy, mean squared radiated energy and spontaneous power spectrum in a power series expansion of the equations of motion in a free-electron laser," *Nuovo Cim. B*, vol. 50, no. 1, pp. 64–88, 1979, doi: 10.1007/BF02737622.

[18] K.-J. Kim, Y. Shvyd'ko, and S. Reiche, "A Proposal for an X-Ray Free-Electron Laser Oscillator with an Energy-Recovery Linac," *Phys. Rev. Lett.*, vol. 100, no. 24, p. 244802, Jun. 2008, doi: 10.1103/PhysRevLett.100.244802.

[19] R. R. Lindberg, K.-J. Kim, Y. Shvyd'ko, and W. M. Fawley, "Performance of the x-ray free-electron laser oscillator with crystal cavity," *Phys. Rev. ST Accel. Beams*, vol. 14, no. 1, p. 10701, Jan. 2011, doi: 10.1103/PhysRevSTAB.14.010701.